Cobalt Decorated Hierarchical Porous Carbon Spheres for High Sulfur Loading Lithium Sulfur Batteries

by

Ruohan Jiang

A thesis
presented to the University of Waterloo
in fulfilment of the
thesis requirements for the degree of
Master of Applied Science
in
Chemical Engineering (Nanotechnology)

Waterloo, Ontario, Canada 2019

Author's Declaration

I hereby declare that I am the sole author of this thesis. This is a true copy of the thesis, including any required final revisions, as accepted by my examiners.

I understand that my thesis may be made electronically available to the public.

Abstract

With the growing need of energy storage devices, the market shows a strong requirement of lithium-based batteries. Nowadays, Lithium ion batteries (LIBs) are dominating the battery field because of its high energy density and low safety risks. However, the energy density of LIB is pushed to its principle limitation. To further improve the battery performance, another new battery mechanism has been developed. Lithium sulfur batteries (LSB) have four times higher energy density of LIBs in principle. LSB are considered as the next generation of batteries in electric vehicles and portable devices by many scientists and material engineers.

In another hand, there are still a lot of obstacles on lithium sulfur technology. Firstly, sulfur is an insulator, so it must be mixed with other conductive supporters to form the electrode which decrease the energy density respect to total weight. During the oxidation-reduction reaction, soluble polysulfide is generated as an intermediate. It is soluble in electrolyte and diffuse through the separator toward the cathode and react with lithium. In the charging process, the Li_2S on the cathode cannot be reduced which is a waste of the active material. The Li_2S layer form on anode also deactivated the lithium plate and cause the capacity fading.

In this project, cobalt decorated hierarchical carbon sphere (CZ/HPC) is designed to overcome these obstacles. This spherical material has three types porous structure including 3nm mesopores, 150 nm middle-size macropores and large carbon bubbles which is around 2 μm. Spherical structure can provide good ion transfer and high conductivity at the same time. Large carbon bubbles and middle-size macropores provide high sulfur loading in the electrode and the mesoporous structure increase the utility of

the sulfur which reflect to high specific capacity. The size of the particle is around 3.5 μm, and larger size of particle made it easier to form thick electrode. The sulfur loading of the battery is over 10 mg/cm^2 and the weight percentage of the active material in the cathode is 72.3% which provide excellent energy density of the battery. To limit the shuttle effect, cobalt nanoparticles generated by calcination of ZIF-67 particles, as an effective polysulfide absorption material, is synthesized on the carbon sphere. Spray dry, which is widely used in the industry, is chosen to synthesize CZ/HPC, and the price of the precursor is relatively cheap that gives CZ/HPC a potential of commercialize.

Acknowledgement

I would like to appreciate Prof. Zhongwei Chen for the chance of study, experiment resources, helpful supervision and tremendous support to my master study. Also, I would like to thank Dr. Yining Zhang who gave me many advices, huge support and suggestions.

I would like to thank my colleagues including Dr. Matthew Li, Ruiling Liang, Dr. Zhaoqiang Li, Dr. Gaoran Li, Dr. Fei lu, Xiaoyuan Dou, Yue Niu, Maiwen Zhang, Abel Sy, and other friends for their helps.

Many thanks to my parents and all the family members for their support and consistent love.

Table of Contents

List of Figures

List of Tables

List of Abbreviations

EV	Electric Vehicle
LIB	Lithium Ion Battery
NMC	Lithium Nickel Manganese Cobalt Oxide Battery
LFP	Lithium Ion Phosphate
NCA	Lithium Nickel Cobalt Aluminum Oxide Battery
LSB	Lithium Sulfur Battery
DOL	Dioxolane
DME	Dimethoxyethane
TiO_2	Titanium Oxide
rGO	Reduced Graphene Oxide
g-C_3N_4	Graphitic Carbon Nitride
SiO_2	Silicon Oxide
P_2O_5	Phosphorous Pentoxide
MOF	Calcination of Metal Organic Framework
ZIF	Zeolitic Imidazolate Framework
Co-C	Cobalt@Carbon
HPC	Hierarchical Porous Carbon
NaCl	Sodium Chloride
CZ/HPC	Cobalt Decorated Hierarchical Porous Carbon Sphere
$Co(NO_3)_2 \cdot 6H_2O$	Cobaltous Nitrate hexahydrate
MeOH	Methanol
SEM	Scanning electron microscopy

XRD	Transmission electron microscopy
ICP	Inductively coupled plasma atomic emission spectroscopy
BET	Brunauer–Emmett–Teller
BJH	Barrett-Joyner-Halenda
DFT	Density Functional theory
CV	Cyclic voltammetry
EIS	Electrochemical impedance spectroscopy

1. Introduction

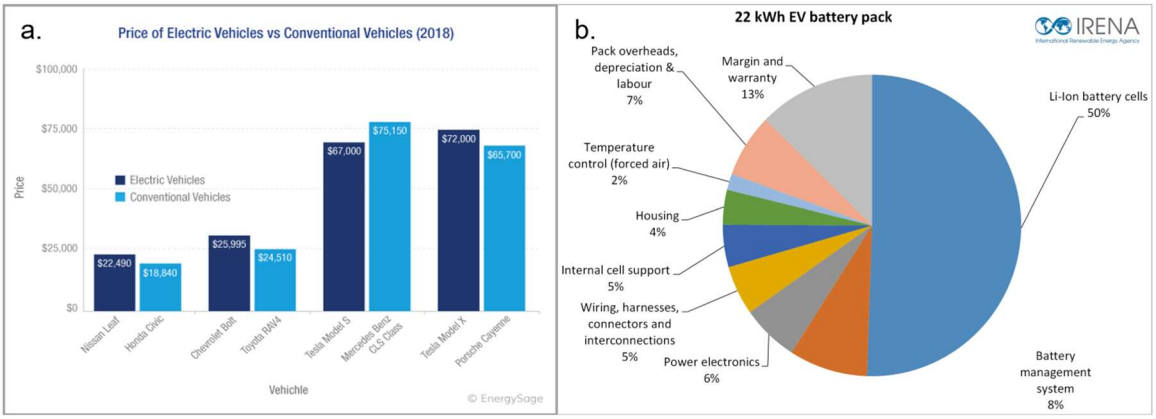

Figure 1: Current situation of EVs in the market.[1] (a). Price of EVs compare with conventional vehicles. (b). market of different kinds of EV battery packs.

The search for clean energy becomes popular due to the environmental problems all around the world. Global warming is a serious issue for the whole world with the global temperature increasing more rapidly than before. To slow down the pace of the climate change, many countries managed to use some sort of renewable energy to replace the gasoline. Many European countries plan to ban combustion engines in 10 to 30 years. For example, France announced plans in 2017 to ban all diesel and gasoline cars by 2040 and further becoming carbon-neutral by 2050. Norway, as a leader in electric-vehicle (EV) technology, has already taken steps towards this cause. The sale of fossil cars in Norway has dropped relative to the Tesla model 3, which has become popular, setting a sales record in March 2018.[1] In addition, only around 40% of the registered cars in March 2018 are still using combustion engine. Although the EVs starts to be very common in Europe and North American, there are still many problems in the field of electrochemical batteries that need to be solved. Firstly, the safety of batteries is the main issue that prevent consumers from driving zero-emission vehicles. After the widely publicized

battery explosion accident of the Samsung Galaxy note 7, the credit of batteries went into another trough. As for the economic concern, the cost of EVs needs to be comparable with traditional vehicles. Fig. 1 (a) shows the cost break down of the EVs and the price of batteries is the determinate factor of the total car price. Manufacturing companies desperately need to find a new generation of battery which cost less while maintaining vehicle performance. Fig. 1 (b). compares the price of the tradition cars and EVs at the vehicle class and most of the EVs cost more. Although the fuel economy of electric vehicles is usually better than combustion engines, the price of the vehicle itself is still too high. In the last ten years, most of the EV companies need to rely on the support from the government to be profitable. For example, the United Kingdom government tried to push the development of EVs by giving up to 4500 pounds of purchase incentives to the drivers. Furthermore, the driving range of EVs also needs to be improved. The median driving range of gas cars is around 410 kilometres which is difficult to reach for most EVs. Although some of the EVs, Tesla Model S, can reach 450 km range after a full charge, people are still scared of driving long distances with an EV because of the fear of running out of power (range anxiety). Also, fully charging an EV usually takes more than an hour which also prevents people from driving electric cars for a long distance. In conclusion, the performance problems of next generation batteries are the main obstacle for EV development and needs to be solved before the fossil cars totally retire.

1.1. Lithium ion batteries

Because of its relatively high capacity and long cycle life, lithium ion battery (LIB) is the most popular battery in people's life. Lithium ion batteries have quickly

occupied the market since its first commercialization. Graphite is used in most of the anode material, and the half reaction is

$$LiC_6 \rightarrow Li^+ + C_6 + e^-$$

The mechanism of this reaction is injection of the lithium ions into the inter layers of graphite. Carbon acts as a framework of the electrode which limits the volume expansion between charge and discharge. As for the anode material, different materials were chosen considering its cost, cycle life and energy density.

In 1996, LIB is developed by Goodenough, Akashaya and their coworkers while Lithium ion phosphate (LFP) electrode is used as the cathode material. The cycle life of this kind of battery is relatively long and 75% of capacity can be maintained after 8000 cycles. The voltage the battery is also very stable which stay close to 3.2 V during discharge. Another advantage of LFP is the low price. Ion is abundant on the earth which low down the material cost. The thermal stability and reliable performance made the battery has a large field of applications. In this case, the LFP is mostly used as for backup power supply or large-scale stationary applications. However, the energy density of LFP is only 90 Wh kg^{-1} due to its low working voltage.[2]

NMC is the most widely used commercialized battery in the recent 10 years. The ratio of nickel, manganese, and cobalt can be adjusted for different requirement. For example, 5:2:3 ratio (nickel, cobalt and manganese respectively) provide long cycle life but lower energy density. 8:1:1 ratio has highest capacity, but the stability and safety issue limit the application of this kind of battery. Researchers also use aluminum instead of manganese to form Lithium Nickel-Cobalt-Aluminum oxide battery (NCA). This kind of battery has high energy density and relatively long cycle life. However, the synthesize

of the battery needs crucial conditions and some high-end techniques, so the price of NCA batteries is higher than NMC batteries.[3]

1.2. Lithium sulfur battery

In order to increase the specific capacity and lower the cost, lithium sulfur battery (LSB) became a hot topic in the battery field.[4] The LSB entail the reaction between lithium and sulfur to form lithium sulfur. The reaction is a step reaction and polysulfide are generated as the intermediate. The mechanism is shown below:

$$Li + 2S \rightarrow Li_2S$$

$$S_8 \rightarrow Li_2S_8 \rightarrow Li_2S_6 \rightarrow Li_2S_4 \rightarrow Li_2S_3 \rightarrow Li_2S$$

LSB batteries had been largely underestimated for over 200 years and proved to be impractical by many researchers because sulfur is insulator which means the electrons are not able to pass through the electrode. In this case, only a small amount of sulfur contributes to the capacity of the battery. However, L. Nazar's group provided an idea in 2009 which uses conductive carbon material and sulfur together to form the electrode.[5] This method overcomes the obstacle of the nonconductive electrode and the use of conductive host material give a new life of LSB. By using mesoporous carbon, the battery gives around 1000 mAh g^{-1} of specific capacity but faded quickly after 50 cycles. This phenomenon is mainly caused by several reasons. First, there is about 80% of volume change before and after charging. The volume expansion of sulfur to lithium sulfur can lead to the disconnection of the active material with the conductive host material. The dissociated lithium sulfide is not able to contribute to the capacity which leads to battery fading. Second, polysulfide is soluble in the commonly used organic

electrolyte, for example, the mostly used DOL/DME based electrolyte in LSB.[6,7] These intermediates may diffuse through the separator and react with lithium metal on the surface of the anode. As the diffused active material is not in contact with the cathode, these polysulfide particles do not contribute to capacity. Also, Lithium sulfide generated on the surface of the lithium electrode deactivates the lithium electrode, increasing impedance and lowering the overall output voltage of the battery. This phenomenon is called 'shuttle effect', and one of the main goals of the researchers is to limit the diffusion of the polysulfide and reduce the fading rate of the battery.[8,9] Another limitation of the lithium sulfur batteries is the self-discharge, and the mechanism of this phenomenon is still now clear. Because of the high capacity and short cycle life, commercialized LSBs are mainly used in space industry.

In conclusion, the advantage of LSB is its high theoretical capacity and low cost. 1675 mAh g^{-1} of theoretical capacity makes LSB a potential power supply of EVs. The cost of LIB is increasing because of the increasing price of cobalt.[10,11] While there are some studies looking into Co free metal oxides, this type of material produces another suite of problems.[12] Compare with cobalt, sulfur is abundant on the earth which gives LSB price advantage. These years, commercial LSB is mainly used in aerospace/drone field because of its short cycle life and the use of lithium metal.

1.2.1. Common strategies for LSB

To solve these problems, scientists mainly focus on several aspects. For the cathode host material, high pore volume is necessary to increase sulfur loading. Porous carbon material is the most wildly used host materials in sulfur anode due to its low

density, which maximize the sulfur loading, and overall conductivity. In 2009, Ji *et al.* firstly demonstrated functional LSB by using ordered carbon nanostructure as host material.[5] Over 1000 mAh g^{-1} of specific capacity is reached and 80% of capacity remains after 20 cycles. Since then, LSB battery starts to be a hot topic for all the energy storage related researchers all around the world which led to rapid development of LSB. For example, Sohn and coworkers used aerosol-assisted method to synthesize several kinds of porous spherical carbon material. The pore size and the pore volume can be adjusted, and the battery performance mainly depends on the porous volume of the host material. Around 1200 mAh g^{-1} of first cycle specific capacity is achieved under 0.1C charging rate and as high as 2C of charging rate is achieved.[16] Jayaprakash introduced a method using silica hard template to generate hollow carbon materials which further enlarge the pore volume. The battery performance significantly increase with the capacity remains 94% after 100 cycles under 0.5C.[17] Evers provided another strategy where graphene was used as an envelope to pack the sulfur particles to reach high sulfur loading in the electrode.[18] As high as 87% of active material is loaded in the electrode and around 700 mAh g^{-1} of specific capacity is reached. However, cycle life of this battery is only 50 cycles and the capacity faded to 500 mAh g^{-1}. Zhang designed a mesoporous carbon fiber material with microporous shell. The mesoporous structure increases the sulfur loading and the microporous shell significantly restrict the shuttle effect while increasing the coulomb efficiency at the same time.[19] The battery performance is outstanding. More than 1200 mAh g^{-1} of specific capacity is reached on the first cycle and more than 800 mAh g^{-1} of specific capacity is remained after 100 cycles under 2C charging rate. In

addition, the battery also shows excellent performance under high rate discharging where the specific capacity is over 750 mAh g^{-1} under 4C.

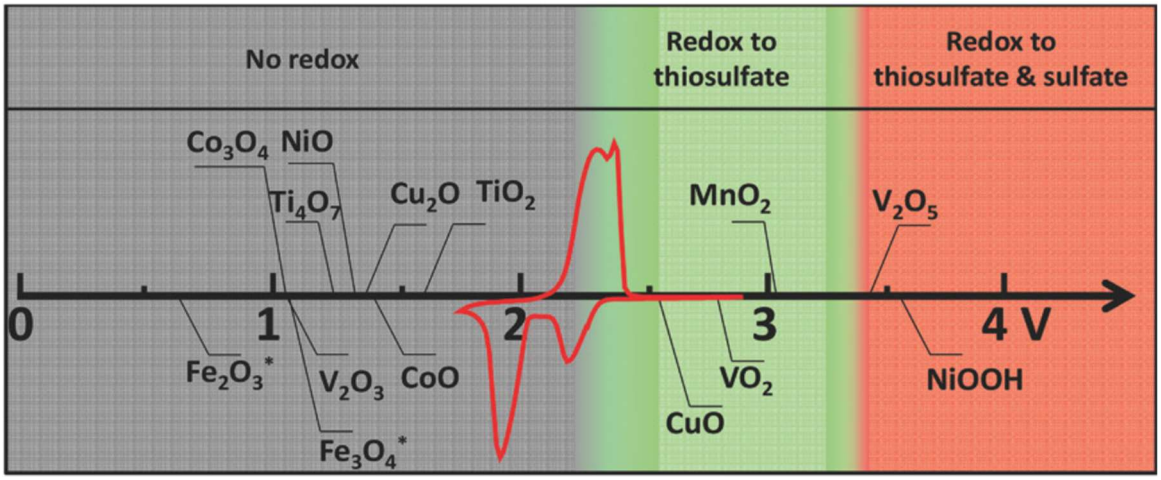

Figure 2: Redox potential of different kinds of metal oxide with polysulfide.[20]

Liang *et al*. studied the sulfur absorption of several kinds of metal oxide and used XPS methods to prove their results. The redox potential against Li/Li+ of several kinds of metal oxides are shown in Fig. 2 where the compounds in the green box can react with polysulfide and shows strong PS absorption ability.[20] Luo *et al* mates provided a double shell spinel nickel-cobalt oxide sulfur host material where nickel, cobalt and oxygen element is normally distributed in the whole structure. The charging rate can reach as high as 5C and the battery can remain more than 700 mAh g^{-1} of specific capacity after 800 cycles.[21] The use of carbon material as conductive support increases the conductivity of the electrode where the addition of metal oxide strongly improved the battery performance, especially the cycle life of LSB.

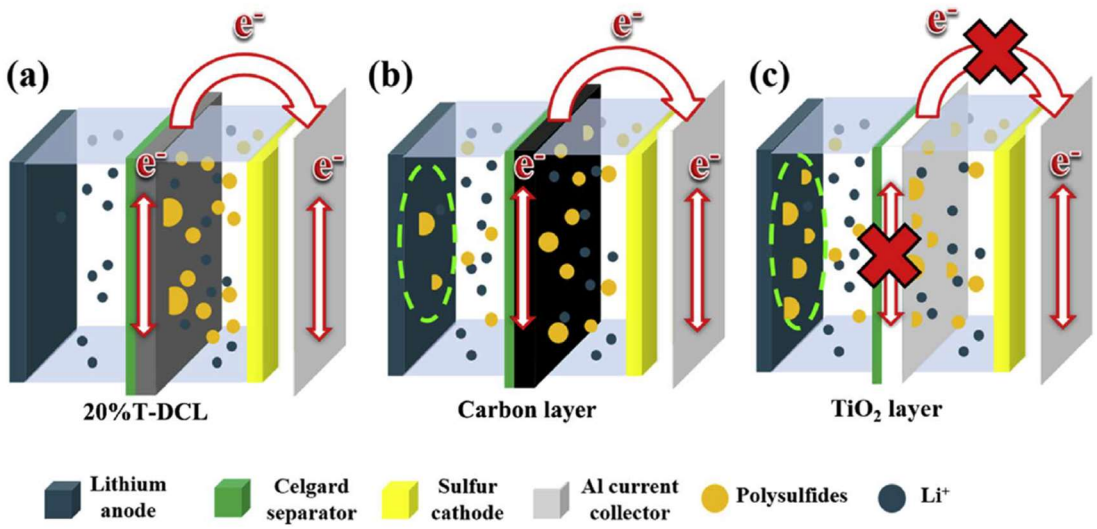

Figure 3. Mechanism of different separator coating strategy.[23] (a). coating the separator with TiO_2 doped carbon material. (b). carbon coating on the separator. (c). TiO_2 layer on the separator

On the other part of the battery, the separators have also drawn much attention as its modification can be used to restrict the shuttle effect. Zhang and coworkers coated the separator with aluminum oxide by doctor blade coating method.[22] The porous layer limits the contact of polysulfide with the lithium anode which decreased the loss of active material and improved the capacity of the battery after cycles. The specific capacity of battery with regular separator and coated separator is compared and the improvement is significant. Many other novel ideas were produced to limit the shuttle effect. For example, Fig. 3 shows the synergetic mechanism of conductive carbon and nonconductive low pore size layer trapping polysulfide.[23] Titanium oxide (TiO_2) coated separator has lower pore size and higher pore volume which can absorb polysulfide. The conductive layer creates electric field where the negative charged polysulfide ions are forced to diffused back to the electrode. Shao and his coworkers compared these three kinds of separators where the carbon/TiO_2 layer shows the best polysulfide absorption ability indicating the synergetic

effect. The cycle life of the battery using 20% TiO_2 coated separator can be up to 200 cycles.

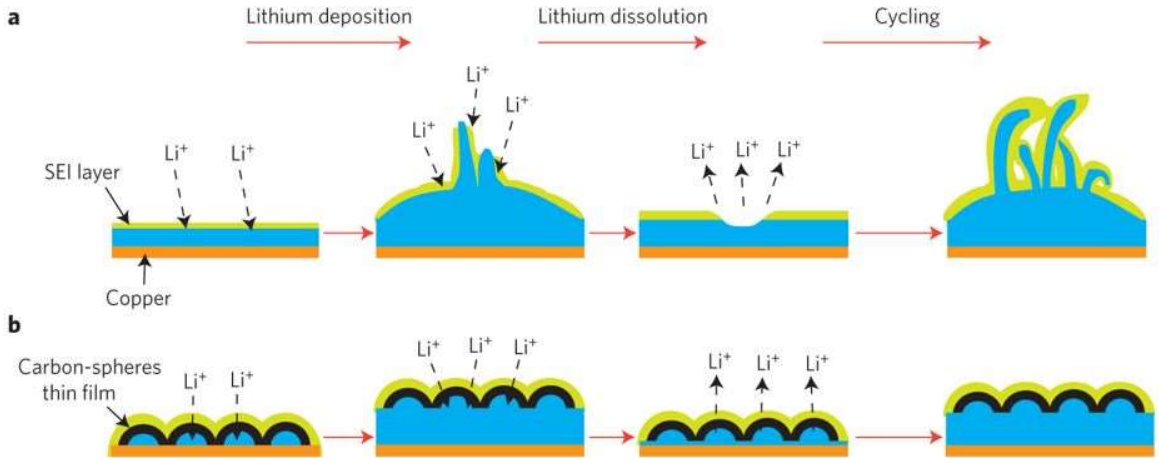

Figure 4: Scheme of carbon-spheres guide the SEI layer to limit the dendrite growth.[24]

As for the anode material, lithium plating is necessary in order to provide practical discharge voltage. However, lithium dendrite is generated during cycles which cause the loss of active material and safety issues. Professor Y. Cui's group provided many strategies to prevent the growth of dendrite. For example, Zheng and coworkers built an artificial SEI layer by coating carbon material on top of the spherical Polystyrene template on aluminum foil.[24] The carbon layer is pushed away from the copper foil during lithium deposition and generates a continuous SEI layer. (Fig. 4) For the lithium plating test, 150 cycles are achieved with nearly 99% coulombic efficiency.

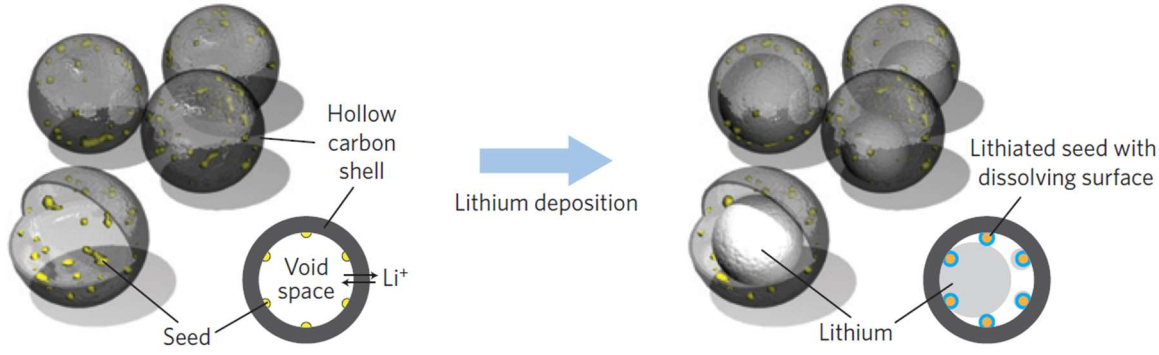

Figure 5: Scheme of gold 'seed' guiding the grow of lithium inside the carbon particles.[26]

Lin and his colleges introduced sparked reduced graphene oxide (rGO) as the host material for lithium electrode. The sparkling reaction is graphene oxide react with molten lithium under sub-ppm oxygen level which increases the spacing of the rGO layer. The top surface of the structure plays a role of artificial SEI layer and other layers support the electrode as a stable scaffold. Sparked rGO has a good lithiophilicity where the molten lithium tends to fill the spacing of the layer structure. Lithium plating test runs for 220 hours and the voltage profile is uniform. Another strategy is to guide the growth of lithium by vertical channel.[25] The host material is made by directly calcinating bass wood. The electrode is made by dipping the host material into the molten lithium and liquid lithium spontaneously fill up the channel due to the capillary force. Another article from Prof. Y. Cui's group demonstrates the lithium deposition on several kinds of metals.[26] The lithium nucleation energy is measured which indicate the lithophilic property. Gold is chosen because of the best lithium wettability and gold nanoparticles are deposited on the carbon hollow material which works as a 'seed' of lithium growing. (Fig. 5) The battery performance is tested by lithium plating where the electrode made by nano-capsules loaded by Au nanoparticles provide over 300 cycles of battery life while the coulombic efficiency is above 98% compare with copper foil electrode which the coulombic efficiency is only around 90%.

1.2.2. Synthesize of Carbon Materials

Carbon material has been used in many aspects due to its unique properties. For lithium sulfur battery, the host material in the cathode is mainly based on carbon. Carbon material has low density and high conductivity and material engineers develop many

synthesize methods to create porous structure. In addition, some nitrogen doped activated carbon is generated by scientists and used in lithium sulfur batteries to achieve high energy density and long cycle life.

Some commercialized carbon material is used in the lithium sulfur batteries. Multi-wall carbon nanotubes are coated with sulfur through capillary action.[27] Graphene is used to pack the sulfur particles or sandwich sulfur layer which increase the overall conductivity of the electrode.[28,29] Ketjen black and Acetylene black are also widely used in lithium sulfur battery due to its high porosity and low resistance.[20-33]

Quan and his coworkers developed graphitic carbon nitride (g-C_3N_4) which has low density and high porosity.[34] From the charge density distribution maps and polysulfide absorption test, g-C_3N_4 also bind with polysulfide which immobilize these soluble active materials. Some other publications also demonstrated same results.[35,36] g-C_3N_4 is synthesized by using silicon oxide (SiO_2) nanoparticles as hard template and cyanamide as precursor followed by a 550 °C calcination. Hard template can provide uniform size and shape of porous structure, but hydrofluoric acid must be used to remove the SiO_2 nanoparticles. Hydrofluoric acid is a highly dangerous contact poison and it can penetrate normal experimental gloves. Due to this toxicity, researchers prefer to use soft template instead. Li *et al.* provided a multi-element doped porous carbon sheet for Li-S battery.[37] By using this novel designed material, the capacity and cycle ability of the cells are largely improved. The porous carbon material is synthesized by mixing Phosphorous pentoxide (P_2O_5) with sucrose followed by 200 °C treatment in a sealed reactor. Sucrose is the precursor and P_2O_5 is a multifunctional soft template which decomposes and dope the carbon sheet with phosphate element.

Ma and his coworkers developed cauliflower-like hierarchical porous carbon/sulfur electrode for primary lithium sulfur battery.[38] Gelatin is coated on commercialized Ketjen black porous carbon material and recreate nitrogen doped particles with larger diameter. (Fig. 6) The thickness of the electrode is successfully enlarged due to the increasing size of the host material. As primary cell, the loading of the battery is 14 mg/cm^2 which is the highest loading lithium sulfur battery to the best of our knowledge.

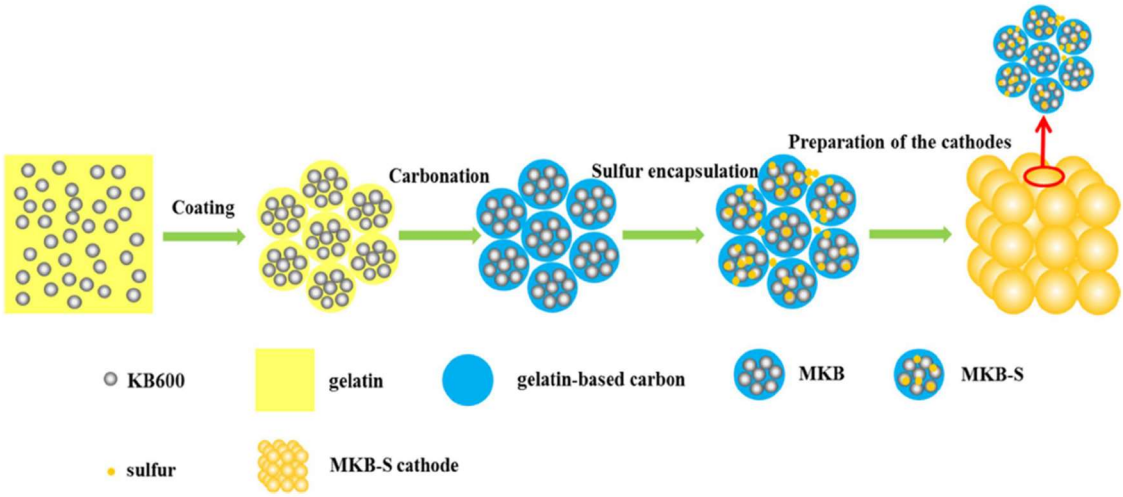

Figure 6: Scheme of the synthesize of gelatin coated Ketjen black particles.[38]

Calcination of Metal Organic Framework (MOF) or Zeolitic Imidazolate Framework (ZIF) is another strategy to synthesize microporous carbon. Direct calcination of some MOFs derives metal decorated microporous carbon materials. Xu developed 3D Zink decorated carbon material by activation and calcination of MOF-5.[39] Zheng *et al.* reported a strategy of calcinate Nickel-MOF to generate nickel doped carbon material in use of Li-S battery.[40] Many other articles reported successfully synthesize of some novel carbon materials by calcination of ZIF-8[41], mesoporous-MOF[42], Multi-wall CNT@MOF-5[43], MOF-525[44], and so on. Li *et al.* demonstrated a synthesize method of using ZIF-67 to

decorate rGO to provide cobalt decorated carbon material.[45] in this article, the excellent polysulfide absorption ability of cobalt@carbon (Co-C) has been proved. X-ray photoelectron spectroscope proved the existence of chemical binding between polysulfide and Co-C.

1.3. Project objective

The proper of this project is to develop a new carbon-based material which has potential to be commercialized for high loading lithium sulfur battery. This material is designed to have hierarchical porous structure where the macropores can increase the loading of the battery and the mesopores limit the shuttle effect and further improve the cycle ability. Characterization of the material need to be done in order to demonstrate the successful synthesize steps and ensure the morphology meet the requirement. Coin cells will be assembled to test the battery performance including the cycle life and the energy density.

1.4. Organization of thesis

The thesis can be separated into 6 chapters. The first chapter introduce the mechanism of lithium ion battery and sulfur battery, the recent research and research milestones of lithium sulfur batteries, and the goal of this project. Chapter 2 introduced the experiment method. Chapter 3 introduce the back ground and principle of the characterization methods. Chapter 4 analyze the result and the experiment data. Chapter 5 is the summary of this thesis and Chapter 6 provide some suggestion of the future research directions.

2. Experiment

2.1. Synthesize of Hierarchical Porous Carbon Sphere (HPC)

140 g of sodium chloride (NaCl) is dissolved in 2 L of water. The solution is heated on the hotplate at 80 °C. 10 g of gelatin is dissolved into the solution while stirring. The solution is feed into the spray dryer by the extrusion pump with a speed of 50 R/min. The fan speed is 100 Hz and the air temperature are set to be 200 °C. The working interval of the deblocker is 8 seconds to prevent the obstruction of the nozzle. The particles are collected from the equipment and followed by a 1000 °C calcination in the furnace for 10 hours in argon environment. NaCl is washed away by water filtration and the material is finally dried in vacuum oven.

Spray dry method is chosen because it is a mature synthesize technique in the industry. With this method, HPC can be easily commercialized and cost of this material is relatively low. NaCl is chosen to be the template because it is a soft template which is easy to remove from the carbon material. In addition, NaCl is cheap and abundance on the earth which make the material friendly to the market.

2.2. Synthesize of Cobalt Decorated Hierarchical Porous Carbon Sphere (CZ/HPC)

CZ/HPC is produced by an insitu-synthesize method. 0.3984 g Cobaltous nitrate hexahydrate ($Co(NO_3)_2 \cdot 6H_2O$) and 0.5248 g of 2-methylimidazole is dissolved in 20 mL of Methanol (MeOH) respectively in two glass vials. 32mg HPC is dispersed in the 2-

methylimidazole solution in the ultrasonic water bath. $Co(NO_3)_2 \cdot 6H_2O$ solution is slowly pour into the solution while stirring on the hot plate for 12 hours. Extra ZIF-67 precursors are removed by centrifuge method. Solid material is separated from the solution by centrifuge and re-dispersed in methanol to rinse off the extra precursors. This step is repeated for 5 times to ensure the all of the $Co(NO_3)_2 \cdot 6H_2O$ and 2-methylimidazole have been removed. Then, the solution is heated to 60 °C to slowly vaporize most of the MeOH follows by a drying process in the vacuum oven for another 12 hours. The material is finally calcinated in the furnace in argon environment for 6 hours under 600 °C. The heating rate is 5 °C per minutes.

ZIF-67 is a hot topic in the research field, but also easy to synthesize. Calcination of ZIF-67 produce cobalt particles which have strong sulfur absorption ability. Insitu-synthesize method aim to anchor the ZIF-67 inside the porous structure on the surface of HPC which create a spherical cobalt layer. While used as the cathode material of lithium sulfur battery, this kind of structure can pack the sulfur and polysulfide in the porous structure and limit the diffusion of soluble polysulfide toward the anode.

2.3. Synthesis of S@CZ/HPC

Sulfur is dissolved in carbon disulfide solution in the glass vial, and CZ/HPC is dispersed into the solution. Carbon disulfide is vaporized in room temperature in the fume hood. The material is grinded and sealed in a glass vial followed by heated under 154°C in convection oven.

2.4. Electrode making

Electrode is synthesized by using LA133 as the binder. S@CZ/HPC and LA133 binder is used in the slurry with a ratio of 85:15. The LA133 is first diluted in water, and S@CZ/HPC is added into the slurry. The electrode is finally made by blade casting the slurry on aluminum foil followed by 60 °C drying process in the convection oven for 12 hours. After that, the electrode is cut to 12 mm diameter's round shape to fit the coin cells. The loading of the electrode is around 4 mg/cm^2 for practical loading and 10 mg/cm^2 for high loading test.

2.5. Battery Assemble

CR2032 coin cells are assembled in the argon environment glove box with both oxygen and water level lower than 0.5 ppm. Lithium plate and Celgard 2325 glass fiber is used as anode and separator. The electrolyte composite includes 1 M LiTFSI and 0.2 M lithium nitrate in DOL/DME with 1:1 volume ratio.

3. Characterization of the materials

3.1. Physical characterization

3.1.1. Scanning electron microscopy

Scanning electron microscopy (SEM) is one of the most useful tools for material scientist to analyze the morphology. Instead of light, electron beams are used to image the small structures. Compare with light, the wavelength of electron beam is much smaller which gives higher resolution and larger magnification.[46] Several kinds of detectors can be used in SEM for different purports. The most used one is secondary electron detector which detects the electron generated from the sample. While the

electron beam hit the sample, some of the electrons on the surface are emit due to the inelastic scattering of primary electrons. This detector is usually used for understanding the morphology of the materials because only the information of the surface structure is collected. Another wildly used detector is backscattered electron detector.[47] The principle of this detector is to collect the reflected or scattered primary electrons. These electrons have higher energy and provide elemental contrast. For example, heavy metal has higher electron density which gives higher scatter angle and higher contrast. In addition, the electron voltage of the primary electron beam is chosen to be 5kV which is as low as possible except for Energy Dispersive Spectroscopy. The low electron energy can prevent penetration of the electrons into the inner layer of the samples.

The sample is prepared by directly deposition on the carbon tape, and Zeiss ULTRA is used to analyze the structure of carbon material. Field Emission Scanning Electron Microscope (FESEMs) is used for S@CZ/HPC imaging because this microscope has better resistance for sulfur.

3.1.2. Transmission electron microscopy

Transmission electron microscopy (TEM) is another important characterization method to identify the morphology of the materials.[48] Compare with SEM, TEM can only provide 2D pictures and the sample needs to be thin enough to allow the electrons to go through. However, the magnification of TEM can is higher than SEM, and the samples do not have to be conductive.[49] The principle of TEM is similar with optic microscope while the only difference is using electrons instead of visual light. The sample is dispersed in acetone by sonication and deposited on copper mesh. Electrons which comes from the

electron gun are focused on the sample by controlled magnetic field. Some of the electrons are absorbed by the sample and the others hit the detector and create image. The variety of electron amount lead to the contract of the image. Normally, the thickness of the sample should be less than 1 micron due to the energy of the electrons because thicker sample would scatter or absorb most of the electrons which result to low brightness of the image.[50]

The TEM data in this thesis is produced by Philips CM 10 TEM with 60 keV electron energy. These TEM pictures prove the successfully synthesize of the material and ensure the morphology which helps to support the mechanism of the carbon-based material working in the battery.

3.1.3. X-Ray Diffraction

X-Ray Diffraction (XRD) analysis is a convenient characterization method which does not affect the structure of the material.[51] The crystal structure can be identified by comparing JDPDS reference and the experiment data.[52] By using the Scherrer equation (Equation 3.1), the average particle size can be calculated. Ƙ is the dimensionless factor which close to 1, β is the peak width at half the maximum intensity, λ is the wavelength of the X-ray, and θ is the incident angle of the beam.[53] The principle of XRD is scatter and diffraction of the X-ray due to the crystal structure. During the test, X-ray with specific wave length is direct to the sample. In our bench top setup, the intensity of the diffracted X-ray is measured as a function of varying incident angle. The reflection of X-ray can be described by Bragg's law (Equation 3.2) where λ represent the wavelength of the incident beam, θ correspond to the beam incident angle and d is the distance of the

spacing of the crystal planes. λ is a constant which determined by the radiation source while n is a positive integer.[54] While the incident angle theta matches the plane spacing d, a peak on the XRD spectrum is going to be generated.

$$\tau = Ƙ\lambda/\beta cos\theta \quad (3.1)$$

$$n\lambda = 2dsin\theta \quad (3.2)$$

The XRD spectrum in this thesis is collected with Rigaku Miniflex 600 X-ray Diffractometer equipped and a Cu Kα radiation source (λ=1.5406Å) with a graphite monochromator. The scan starts from 5 ° to 90 ° with a scan rate of 0.5 °/min. The spectrum is collected to prove the successful synthesis of the material and identify the crystal structure of the nanoparticles. In addition, the particle size is also calculated from the Scherrer equation.

3.1.4. Inductively Coupled Plasma Atomic Emission Spectroscopy

Inductively coupled plasma atomic emission spectroscopy (ICP) is used to identify and measure the amount of metal. The sensitivity of this analyze technique is very high that trace amount of element can be detected. In ICP equipment, the atoms are heated to around 9000 K and the electrons are thermal activated. Argon plasma is generated in the chamber and during the relaxation process, the radiation emitted by the active atoms is detected. The specific metal element can be identified, and the concentration can be measured by comparing the reference.[55]

The ICP data in this thesis is collected from Perkin Elmer Ltd. The cobalt amount in the CZ/HPC is tested to prove the successfully synthesis of the material.

3.1.5. Nitrogen Adsorption-Desorption Isotherms Analysis

Nitrogen adsorption-desorption isotherms analysis is used to analyze the porosity, surface area and pore distribution of the material.[56] With the development of the modern science, material engineers start to design higher surface area and high porosity materials for different purpose. The material is loaded in the chamber under low temperature and nitrogen gas is adsorbed by the surface of the material. The partial pressure of the gas is measured along with the amount of nitrogen gas absorbed. To identify the most essential morphology parameter, Nitrogen adsorption-desorption isothermal curve is normally analyzed by Brunauer–Emmett–Teller (BET) theory,[57] Barrett-Joyner-Halenda (BJH) theory[58] and Density Functional theory (DFT)[59,60] for different reasons. BET theory simulate the surface area of the material while BJH simulation provide the estimate porosity and pore size distribution. DFT theory is normally used to analyze the pores with higher diameter.

In this thesis, BET and BJH simulation is used to analyze the porosity and pore size distribution of HPC and CZ/HPC. Desorption curve is mainly used as the raw data to inject the BET and BJH modulation.

3.2. Electrochemical Characterization

3.2.1. Galvanostatic charge and discharge

Galvanostatic charge and discharge is the basic performance of batteries. Batteries are connected to the Galvanostatic which provide constant current, and the battery charge and discharge in a reset voltage window. At the end of charging or discharging, the current direction is reversed to continue the battery cycle. The voltage profile of the

battery is tested by measure the voltage versus the specific capacity. One or several plateau may show on the curve which represent different step of the reaction. The charge and discharge rate are calculated base on the amount of the active material and the total theoretical capacity. The C-rate is calculated by (Equation 3.3) where I is the current with unit of mA, C is the theoretical capacity, m is the total mass of the active material in the electrode.

$$\text{rate} = \frac{1}{t} = \frac{I}{C \cdot m} \tag{3.3}$$

The cycle life of the battery is tested by continuously charge and discharge the cell with galvanostatic. Coulombic efficiency is the ratio of discharge capacity and charge capacity which is also generated from this test.

In this thesis, New wave battery tester is used to test the lithium sulfur batteries. CR-2032 coin cell is used in the battery assemble step and standard Celgard separator is used in both HPC and CZ/HPC batteries.

3.2.2. Cyclic voltammetry

Cyclic voltammetry (CV) is an analysis method which characterize the electrochemical properties of the batteries. During the experiment, the voltage applied on the battery linear sweep between a pre-set voltage window while the current of the circuit is measured and plotted against the potential.[61] The reduction and oxidation peaks on the plot provide the information of the electrochemical reaction. For example, the position of the peak provides the overpotential of the specific reaction and the peak area present the total capacity of the cell. Multicycle CV also used to show the satiability of the cell and the reversibility of the reaction.

CV data in this thesis is generated by using the Gamry Interface 5000E potentiostat. The CZ/HPC electrode is assembled in CR2032 coin cell and tested under 0.05 mV s^{-1} scan rate. Combine with the galvanic charge and discharge curve, the CV curve is used to identify the reaction of lithium and sulfur.

3.2.3. Electrochemical impedance spectroscopy

Electrochemical impedance spectroscopy (EIS) is used to identify the basic cell parameters. Nyquist plot is normally used in battery field while the frequency response is detected. Alternating voltage is applied to the cell and the numerical value of the potential is separated to real part and image part by using the Euler's formula. In a typical Nyquist plot, the real part is plot on the X axis and the image part is plot on the Y axis. By simulation of this plot, some basic electrochemical properties such as bulk resistance, charge transfer resistance of the redox reaction, interface resistance and Warburg diffusion factor.[62]

The Nyquist plot in this thesis is generated by test the cell on Gamry Interface 5000E potentiostat. The simulation and modeling are finished by using EC lab software.

4. Result and discussion

4.1. Characterization of NaCl@Gelatin

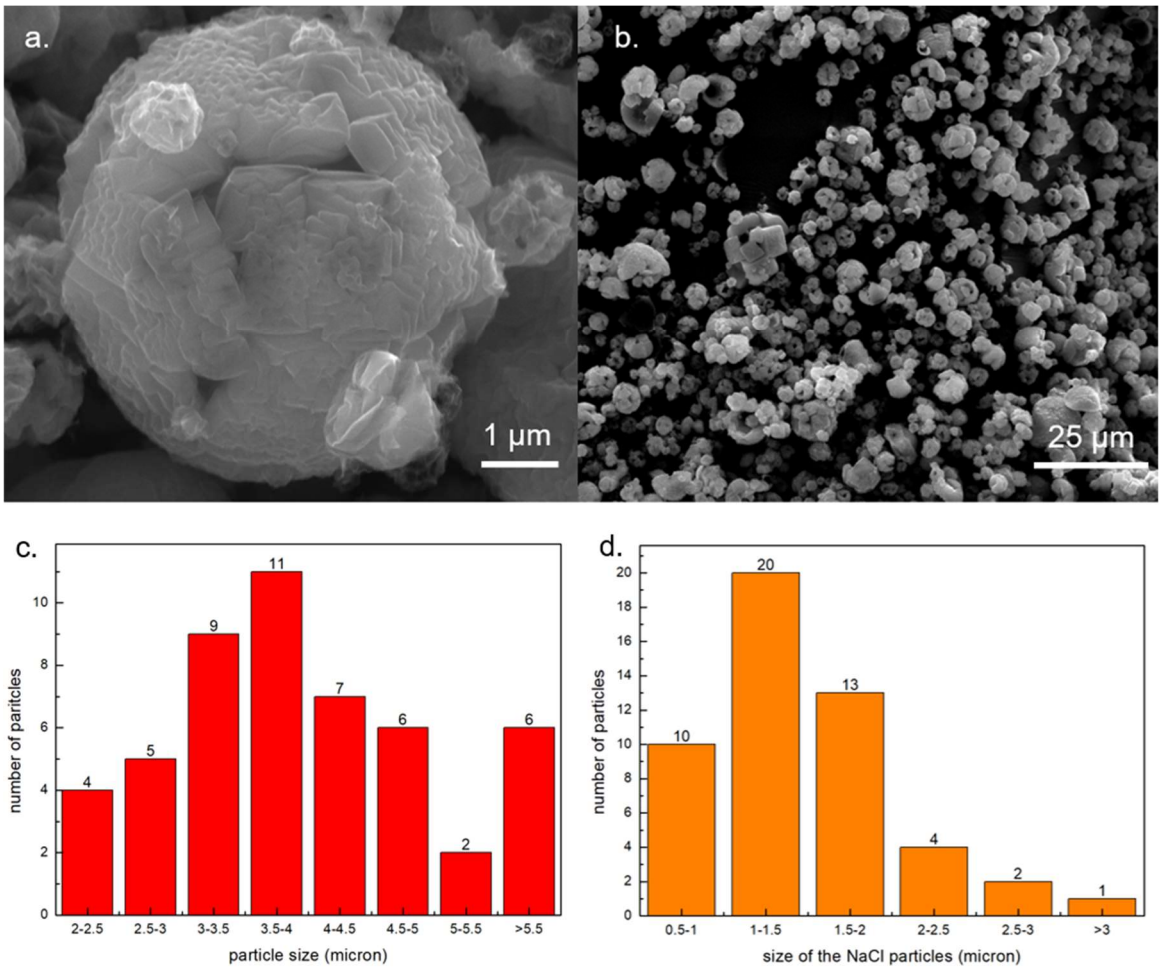

Figure 7: (a),(b). SEM image of NaCl@HPC. (c). Size distribution of NaCl@HPC particles. (d). Size distribution of NaCl templates.

NaCl@Gelatin is successful synthesized through the spray drying method. SEM images of NaCl@Gelatin is shown in Fig. 7 (a)(b). NaCl crystals are covered by gelatin and each NaCl@Gelatin particle contains several NaCl crystals. The particle has a rough surface which consists of middle-size macropores around 100 nm diameter. The size of the NaCl crystals template are around 1-1.5 microns as shown in Fig. 7 (a). NaCl plays an excellent role as template while the shape of the particles is determined by the crystal. In

the synthesis step, NaCl crystalized during the spray dryer process which dry the solution immediately. Under this crucial condition, gelatin and NaCl crystal are well mixed together.

The size distribution of NaCl@gelatin is shown in Fig. 7 (c). The spray drying nozzle sprays the solution into small droplets and the droplets are dried in the drying chamber. The particles are shaped at that moment and the particle size is determined by the size of the droplets. Most of the particles are around 3.5-4 micrometer and some of them is larger than 5.5 microns which may due to the mixing of two droplets during the drying process. The size distribution of NaCl template is shown in Fig. 7 (d) while most of the crystals are from 0.5 to 2 microns.

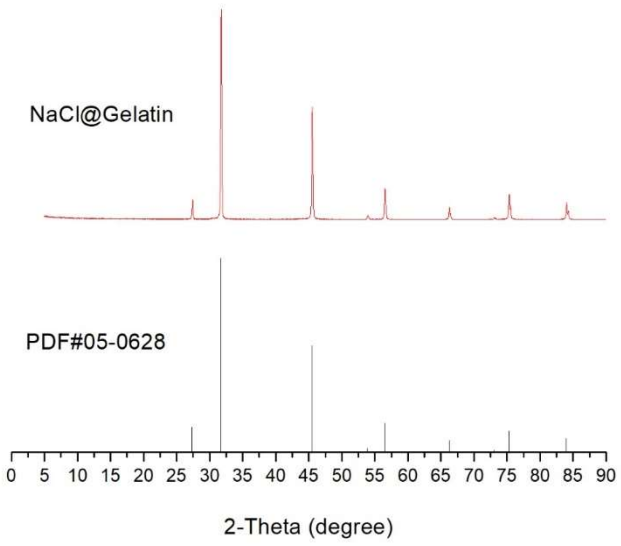

Figure 8: XRD pattern of NaCl@Gelatin.

XRD result of the NaCl@gelatin is shown in Fig. 8 which shows the successful crystallization during the spray drying process. By comparison of the XRD pattern of NaCl crystals and NaCl@gelatin, the NaCl crystal is identified. XRD pattern of

NaCl@gelatin is shown in Fig. where the peaks is located at 27.3º, 31.7º, 45.4º, 53.8º, 56.5º, 66.2 º, 73.0 º, 75.3 º, and 83.9 º which correspond to the crystal plane of (111), (200), (220), (311), (222), (400), (331), (420), and (422), respectively. These positions perfectly match the reference of NaCl and the intensity ratio between peaks also align with the standard PDF card of NaCl (JCPDS#05-06280). This result confirms the successfully crystallization of NaCl during the spray dry process.

4.2. Characterization of HPC

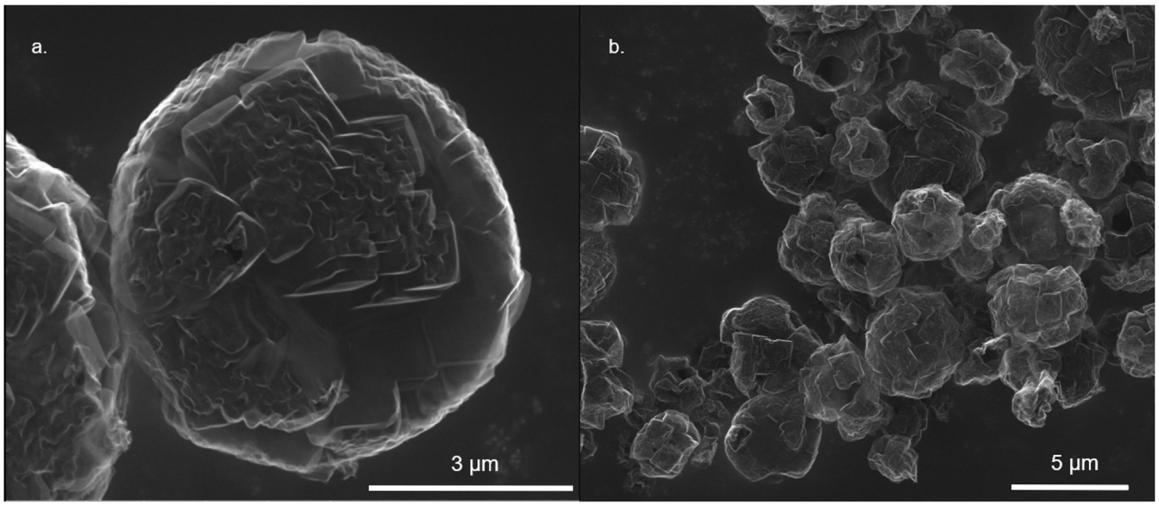

Figure 9: SEM images of HPC.

After the washing step that remove the NaCl precursor, the material was calcined to obtain HPC. Each HPC particle consist three types of pores structure: large carbon bubbles created by NaCl template, middle-size macropores on the particle surface, and intrinsic mesopores due to the calcination of gelatin. SEM pictures of HPC are shown in Fig. 9. The size of the pores is similar before and after calcinations step which indicate that the NaCl crystal is very stable during calcination. The size of the particle is slightly smaller than the NaCl@Gelatin caused by shrinking of gelatin during the calcinations

step. Below 600 °C, the NaCl crystal remains solid phase which strongly stabilizes the structure. Gelatin is carbonized to generate nitrogen doped carbon in this step and the structure is formed. At the second stage of calcinations, which is around 1000 °C, NaCl crystal melted and the material is further carbonized to increase the conductivity. Large size carbon bubbles which created by NaCl crystals are demonstrated clearly for all the particles (Fig. 9 (b)). The bubbles have random shape which create space in between and further increase the porosity. Pores around 100 nanometers are shown on the image. This kind of middle-size porous structure is abundant on the surface of the particle as shown on Fig. 9. (b).

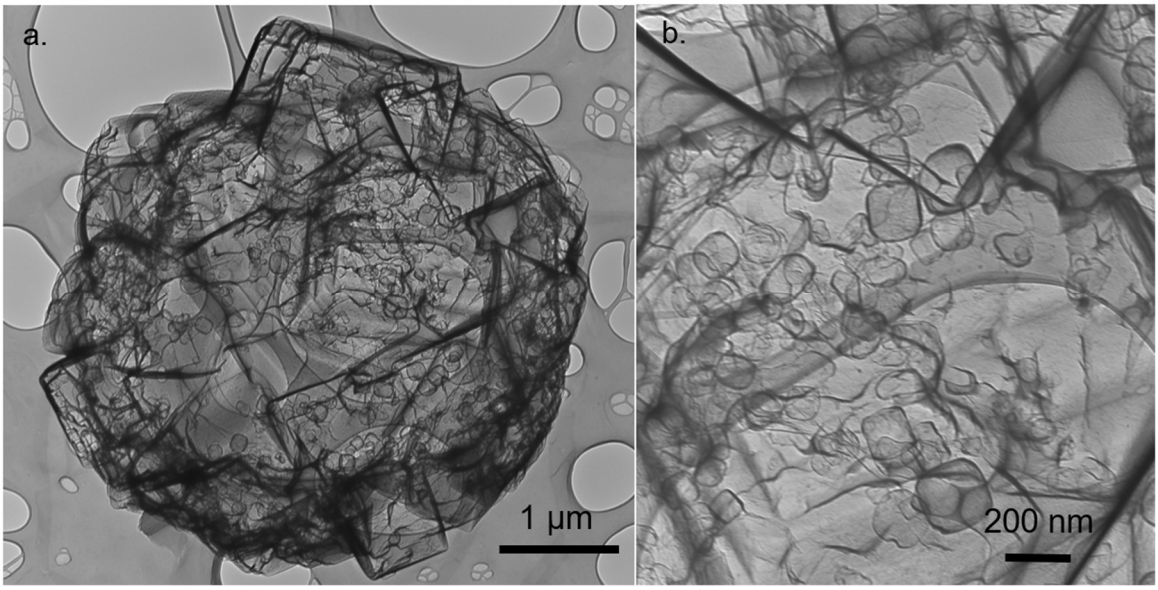

Figure 10: TEM images of HPC.

Fig. are the TEM pictures of HPC. The shell of the particle is very thin which increase the porosity of the material. Corners created by the NaCl crystals are clearly shown on the image. The hierarchical porous structure is clearly demonstrated, and the size of the pores is measured (Fig. 10). Every HPC particles consists several large carbon bubbles with a size of around 2 µm. In addition, large sums of middle-size pores with

diameters around 150 nanometers can also be identified. Further, the pores are distributed among the whole structure, ensuring that the entire structure of the product are fully utilized.

4.3. Characterization of ZIF-67@HPC

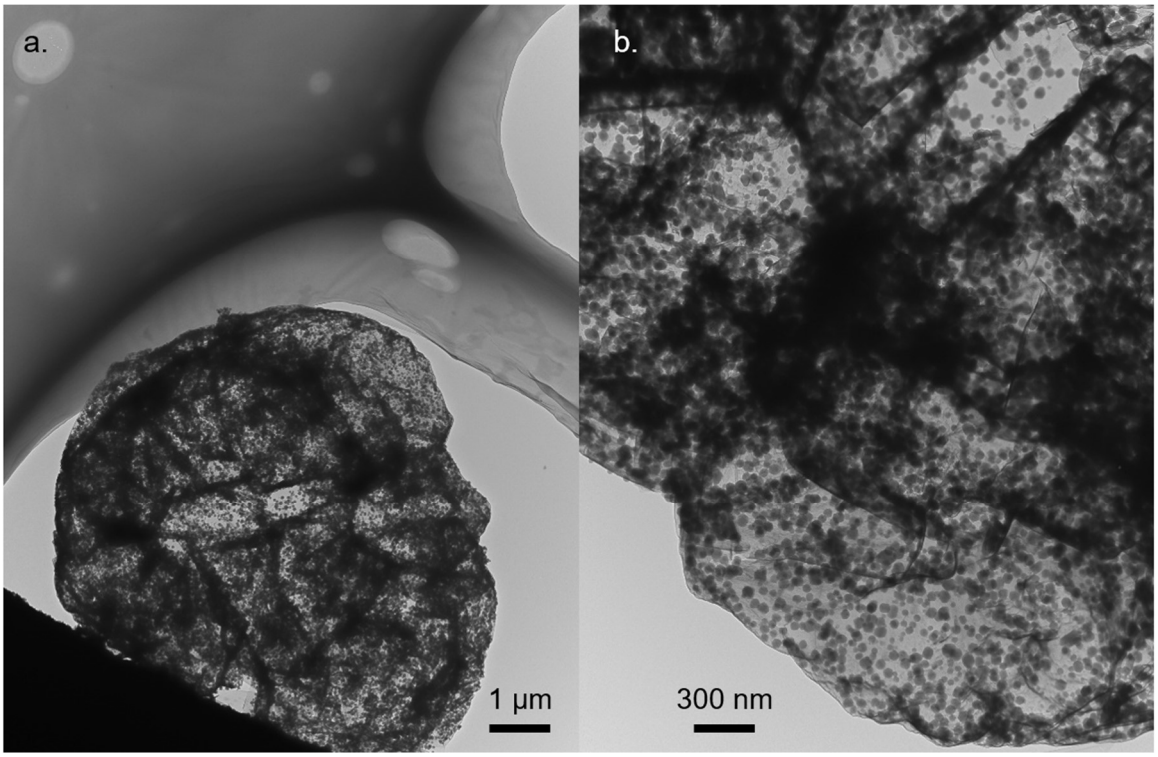

Figure 11. TEM images of ZIF-67@HPC.

ZIF-67 particles were successfully formed on HPC particles through an insitu-synthesize method. The TEM pictures of ZIF-67@HPC are shown in Fig. The ZIF-67 particles are shown in Fig. The identical hexagonal structure of ZIF-67 can be seen in the figure. The particles are well distributed among the whole structure and the synthesis process does not have any influence on the structure of the substrate (HPC) where the size and morphology remain the same. The size of ZIF-67 individual particles are around 40 nm which is relatively small compared with the literature using the same procedure.[45]

4.4. Characterization of CZ@HPC

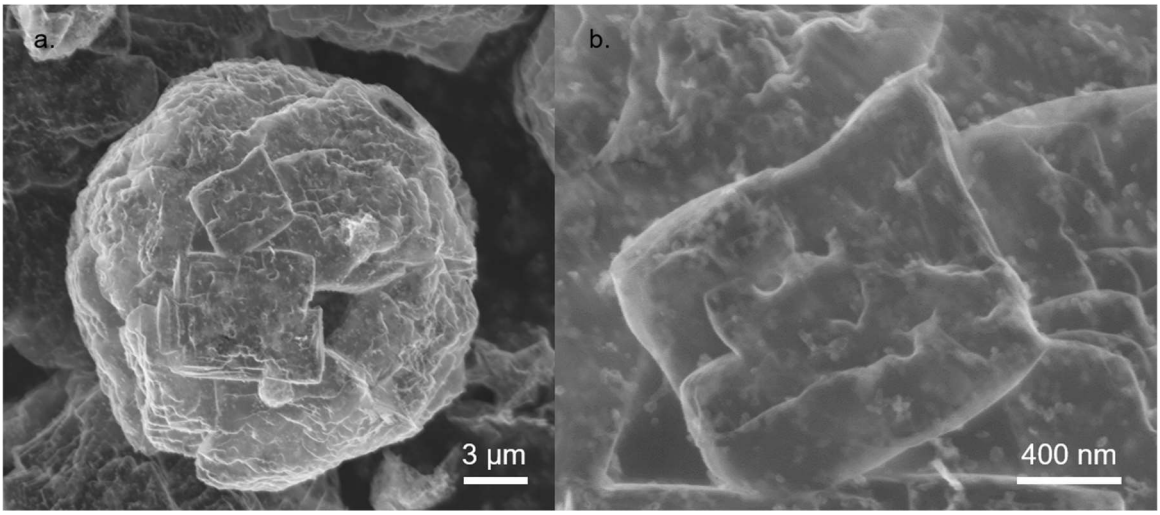

Figure 12: SEM images of CZ/HPC

SEM pictures are shown in Fig. 12. The large pore structure is obvious shown, which proved that the ZIF-67 synthesis step does not affect the structure of the HPC. Carbonized ZIF -67 particles are clearly shown on the surface and the distribution of the particle is very even and there are not any agglomeration appears due to the SEM pictures. Due to the insitu-synthesis method, the carbonized ZIF-67 particles are mostly located in the large pores which are created by the NaCl crystals. While the carbon particles are dispersed in the solution of the ZIF-67 precursors, the middle-size pores on the surface of HPC absorbed most of the cobalt nitrate and 2-Methylimidazole and the reaction happens on the surface of the carbon. The particle size is measured to be 30 nm which is smaller than ZIF-67 particles before calcination. During the 600-degree calcination, the cobalt ions are reduced to cobalt metal and aggregate to form cobalt nanoparticles. 2-Methylimidazole ions decomposed and carbon molecules crystalized with HPC. This is the main reason which lead to the shrinking of the ZIF-67 particles.

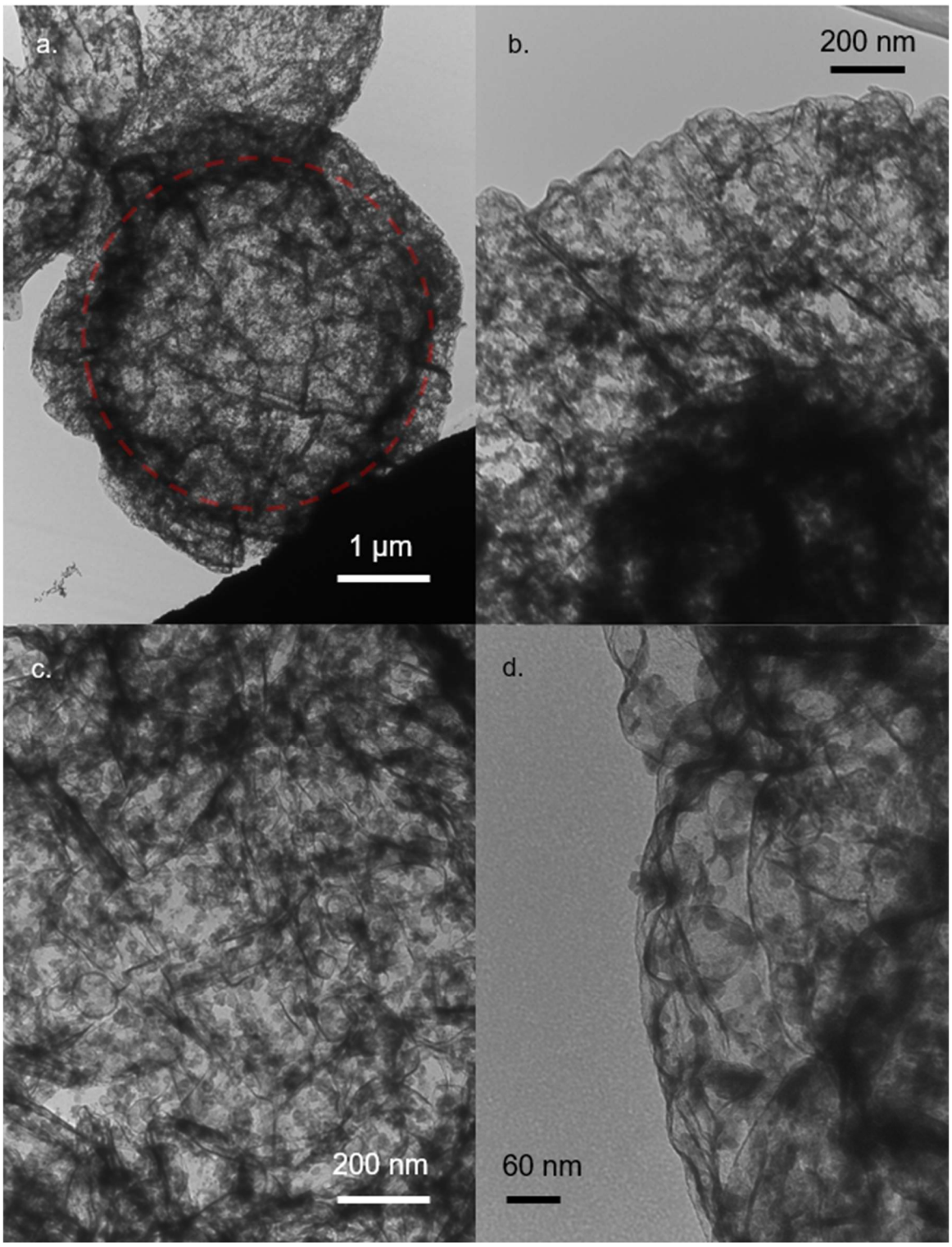

Figure 13:TEM images of CZ/HPC.

TEM of CZ/HPC is shown in Fig. 13. Compare with the TEM pictures of HPC, the addition particles have two different sizes (Fig. 13 (b)(c)(d)). One kind of them is relatively transparent under TEM and the size of them is around 20 nm. These particles are generated by the reduction of 2-Methylimidazole in ZIF-67 and mainly composed of carbon as shown in the SEM figures. During the calcination step, recrystallization of carbon atoms in 2-Methylimidazole leads to shrinking of ZIF-67 particles and form these kind of carbon particles. The other particles are cobalt nanoparticles with smaller size which are darker in the figure. These nanoparticles are formed by aggregation and reduction of cobalt ions and the size of them is around 10 nm. It is also important to point out that the morphology and size of HPC remain the same after the 600 °C calcination process. The size of carbonized ZIF-67 is measured again from TEM images and the result match the SEM result which is around 20 nm. In addition, Fig. 13 (a) shows that the ZIF-67 is mainly anchored in the hollow structure instead of agglomerate in the center of the particle of HPC because the ‘particle ring’ (red circle) shown on the figure.

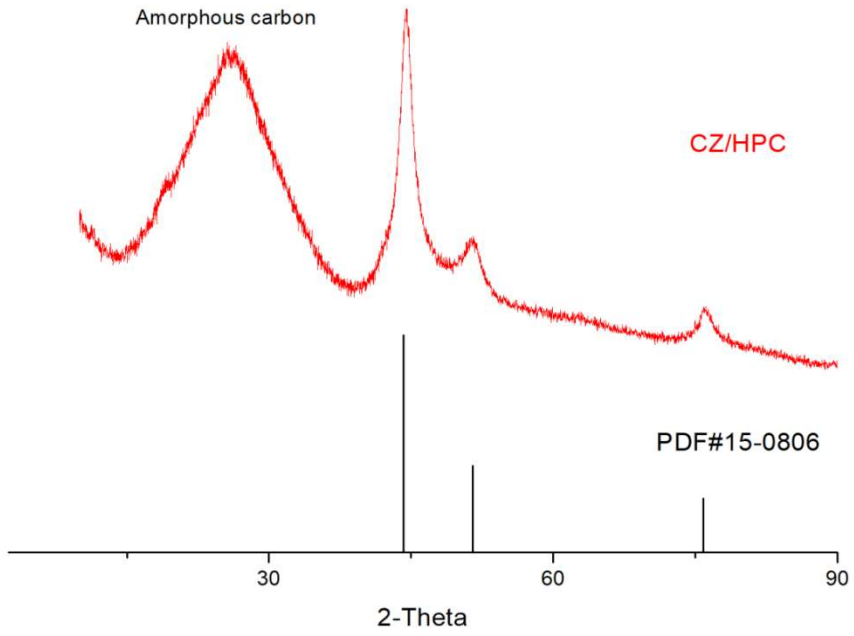

Figure 14: XRD pattern of CZ/HPC and reference.

XRD of CZ/HPC shows the crystal structure of cobalt (Fig. 14). Three sharp peaks located at 44.2º, 51.5º, 75.8º which indicated the (110), (200), (220) crystal plane of cobalt metal, respectively. The wide peak located at around 25.5º attribute to active carbon material and HPC is one of a kind. The size of the cobalt nanoparticles can be roughly calculated from the width of the peak at the half maximum intensity using Scherrer equation. The size of the cobalt nanoparticles is calculated to be around 10 nm while matches the SEM and TEM images.

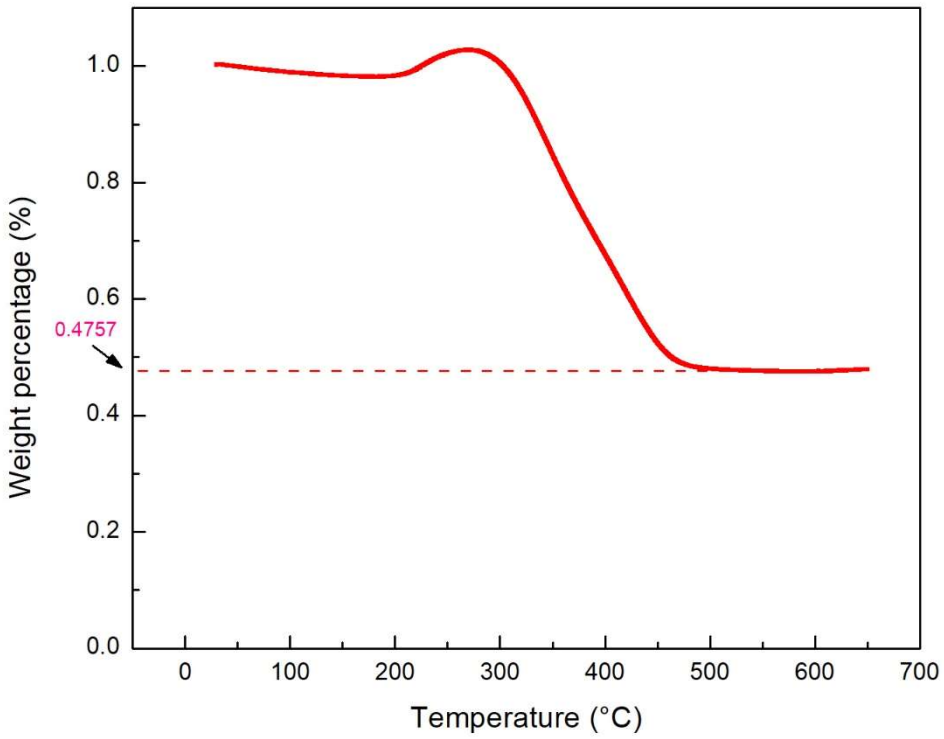

Figure 15: TGA data of CZ/HPC.

TGA data is shown in Fig. 15. The test is under air environment in order to oxidize the carbon material and test the amount of cobalt in the material. At 290 ºC, there is a weight increase which is caused by the oxidation of cobalt to cobalt oxide. After a small increase, the weight percentage curve keeps decrease until 39.05%. In this process, all the carbon material reacts with oxygen yielding gaseous products which are exhausted away from the TGA mass balance. The final material left is Co_3O_4[63] and the weight percent of Co metal in CZ@HPC is calculated to be 34.94% which is close to the Co weight percentage of 33.2% due to ICP test.

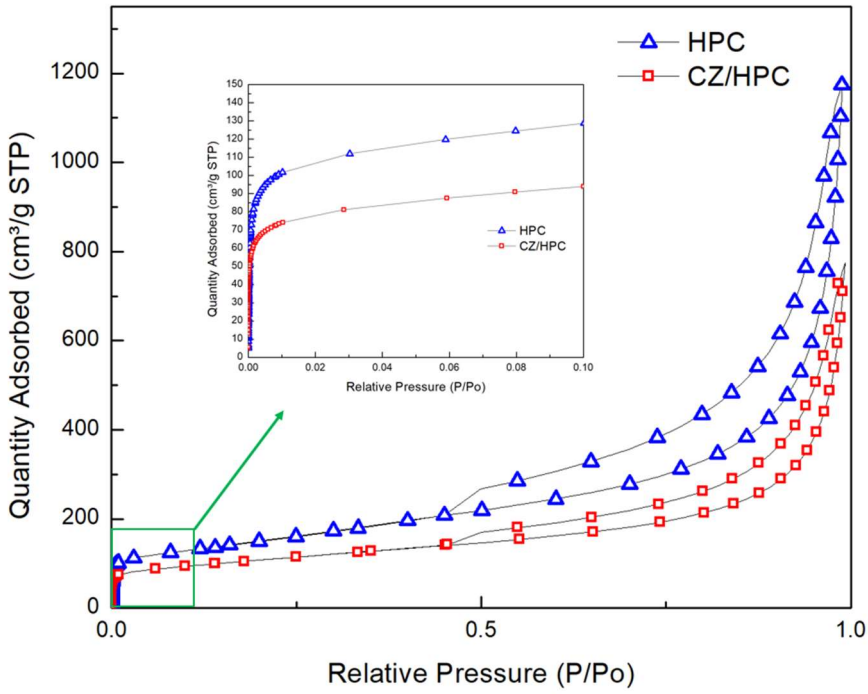

Figure 16: Nitrogen adsorption and desorption isotherm.

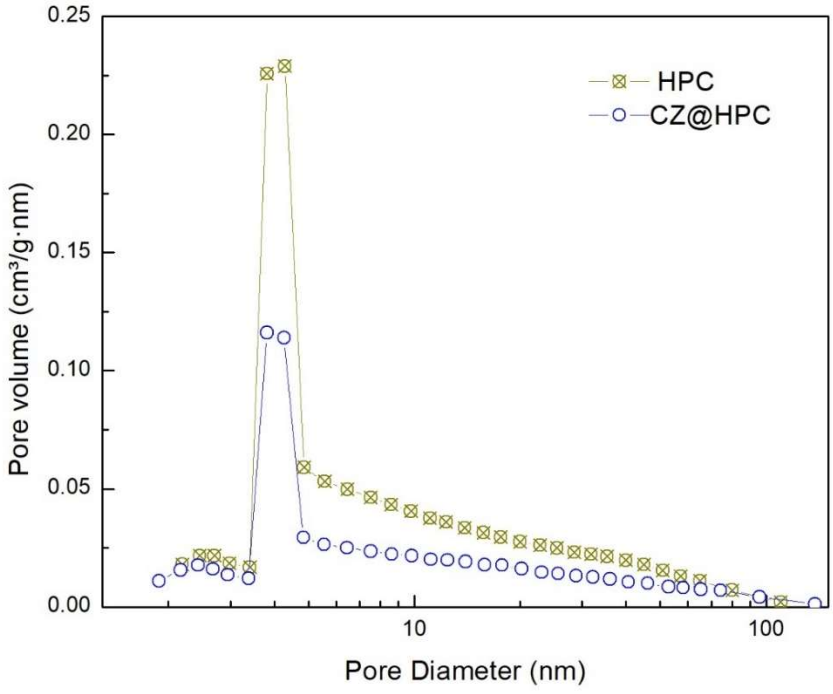

Figure 17: Pore distribution diagram of HPC and CZ/HPC.

Sample	BET surface area	Pore volume	Average pore size
HPC	535.1142 m^2/g	1.743477 cm^3/g	116.3840 Å
CZ/HPC	373.3419 m^2/g	1.127087 cm^3/g	103.4463 Å

Table 1: BET analyze of the nitrogen adsorption and desorption curve.

The nitrogen adsorption-desorption measurement shows the amount of mesoporous of HPC and CZ/HPC. Fig. 16 is the adsorption-desorption isotherms of CZ/HPC and HPC. The acute increase located from 0 to 0.01 P/P_0 suggest the abundance of mesopores in both HPC and CZ/HPC which is created during the calcination of gelatin. Another rapid increase of the curve shows at the position over 0.75 P/P_0 prove the existence of middle-size macropores formed by NaCl template. Fig. 17 the shows the pore size distribution of these two kinds of materials from BET analysis. Table. 1 is the result of BET simulation. HPC mainly consist of mesopores structure (~3 nm) and the pore distribution of CZ/HPC is similar while the pore volume is about half of HPC. By using the BJH simulation, the morphology and porosity is quantitatively demonstrated. The total pore volume of HPC is 1.743 cm^3/g while the surface area is 535.11 m^2/g. The average pore size of HPC is 11.638 nm which is larger than 3 nm because of this material also consist of large amount of microporous structure. Existence of mesopores is essential for cathode material of lithium sulfur material because it has strong sulfur absorption ability. These pores around 3 nm can maximize the use of sulfur and improve the specific capacity of the battery. As for CZ@HPC, BJH surface area is 373.342 m^2/g, total pore volume is 1.127 cm^3/g and average pore size is 10.345 nm for the same reason of HPC. Compare with HPC, the decrease of pore volume is mainly because of the addition of

carbonized ZIF-67 particles. As cobalt nanoparticles are denser than carbon, for the same weight of material, the amount of porous carbon in CZ/HPC is less than HPC, which lead to lower pore volume.

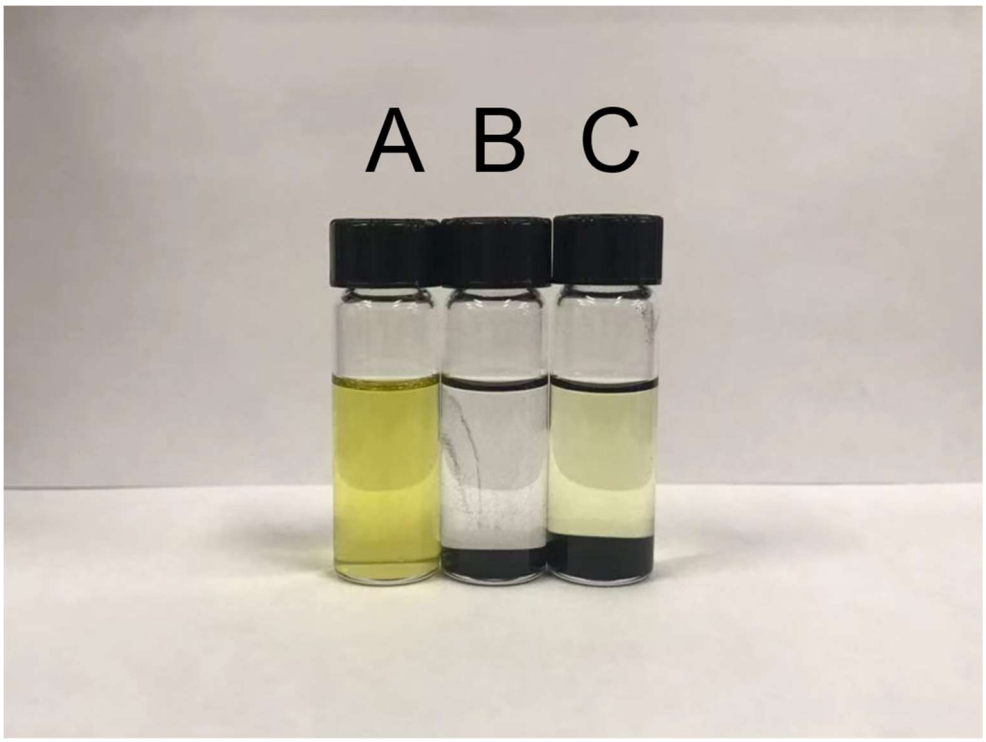

Figure 18: After 72 hours of polysulfide absorption test. A: Reference (1.5mM Li_2S_6 THF solution). B: CZ/HPC. C: HPC.

To test the polysulfide absorption ability of the material, HPC and CZ@HPC is dispersed in Li_2S_6 THF solution. Dissolved polysulfide has a rich absorption spectrum in the visible light regime, giving off orange-yellow colors. Accordingly, the concentration of polysulfide in the solution can be correlated to the degree of light absorption.[64] Same amount of (calculated by the weight of carbon: 3 mg and 4.5mg of HPC and CZ@HPC respectively) material is immerged in 4 ml of 1.5 mM Li_2S_6 THF solution in glove box. As shown in Fig.18, after 72 hours, most of polysulfide is absorbed by CZ@HPC and some of the Li_2S_6 in the glass vial is absorbed by HPC. Compare to HPC, CZ/HPC has

stronger polysulfide absorption ability due to the cobalt nanoparticles.[45] While CZ/HPC based electrode is used in lithium sulfur battery, the shuttle effect can be limited due to the excellent polysulfide absorption ability of the cobalt nanoparticle decorated material.

4.5. Characterization of S@CZ/HPC

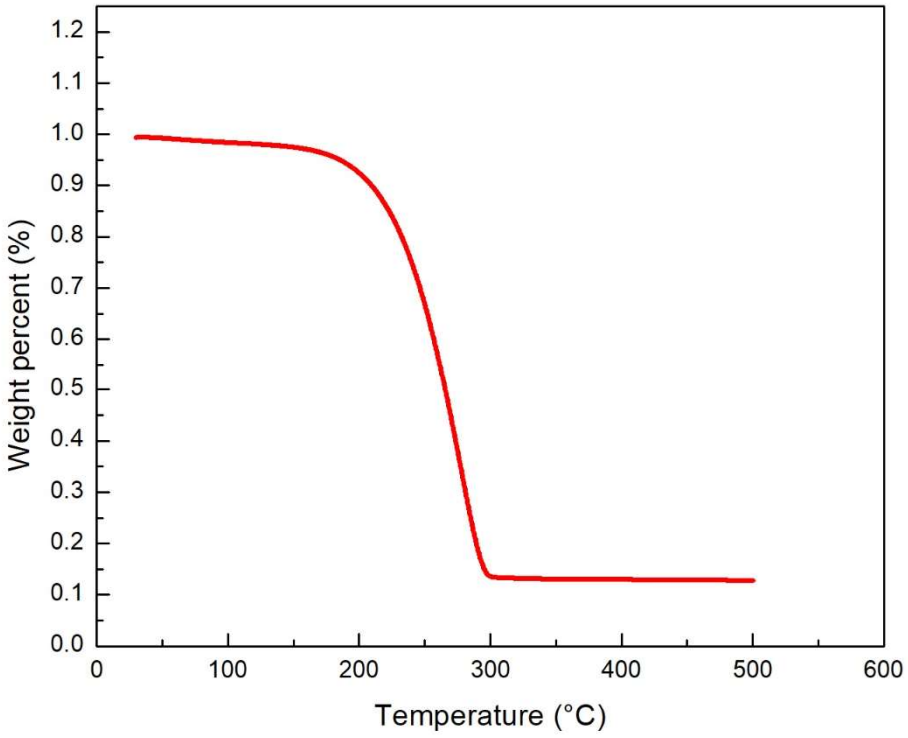

Figure 19: TGA data of S@CZ/HPC.

Sulfur, as the active material of the battery, is dissolved in CS_2 and absorbed by CZ/HPC to form S@CZ/HPC. The amount of sulfur in S@CZ/HPC is tested by TGA in nitrogen environment. During the test, sulfur vaporized, and the total weight decrease to 14% after 400 ºC. The result is close to the target sulfur loading of 85% sulfur in S@CZ/HPC. (Fig. 19) It should be noted that 85% sulfur loading is very competitive

among literature. Most work uses 70-80% which ultimately reduces the effective energy density of the cell.[65-68]

4.6. Battery test

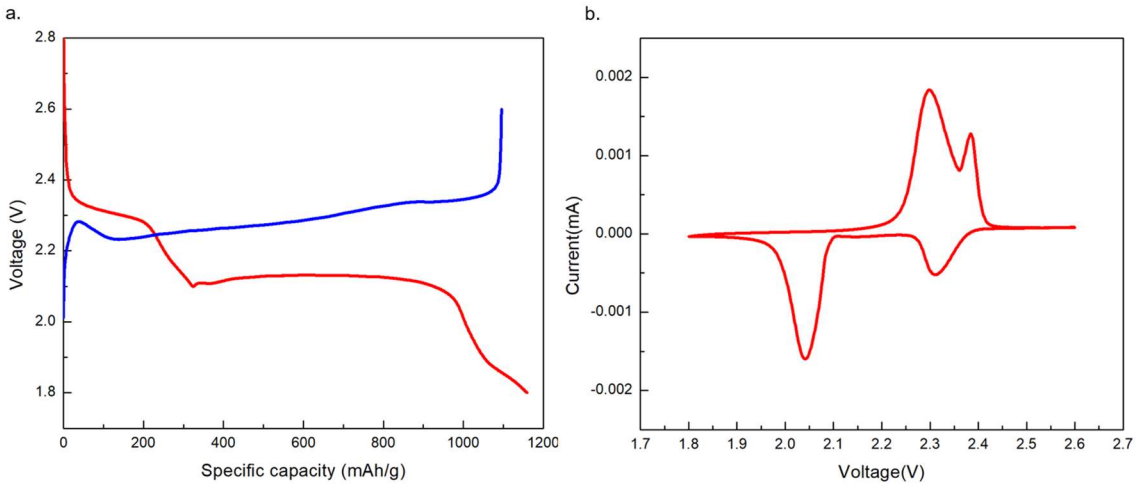

Figure 20: (a). Galvanostatic charge and discharge curve of CZ/HPC coin cell. (b). CV profile of CZ/HPC coin cell.

The sulfur amount in the electron is 72.2% (85% of sulfur in the host material times 85% S@CZ/HPC in the electrode) of weight which is higher than nearly all the other reported results.[69] The high percentage of nonconductive sulfur in the electrode dramatically increase the energy density of the battery but decrease the electronic conductivity and ion transfer ability. However, the batteries still demonstrate good specific capacity, relatively long cycle life and high rate resistance. Fig. 20 (a) shows the galvanostatic charge and discharge curve of the lithium sulfur battery based on S@CZ/HPC electrode. The charging rate is set to be 0.1C, and the voltage window is between 1.8V and 2.6V. Two significant plateaus locate at 2.3V and 2.1V which show on the discharge curve represent the multistep reaction of lithium with sulfur. The first plateau corresponds to reduction of sulfur to Li_2S_6 or Li_2S_8, while the second plateau

relate to further reaction of polysulfide with lithium ions to Li_2S. Similar result is also obtained from the CV curve of the battery, confirming the standard behaviors of lithium and sulfur reaction in the system (Fig. 20 (b)). As shown, the two peaks located at 2.3V and 2.36V represent the sulfur to polysulfide reaction and polysulfide to Li_2S reaction respectively. The separation of these two peaks prove the excellent ion transfer ability in the electrode.

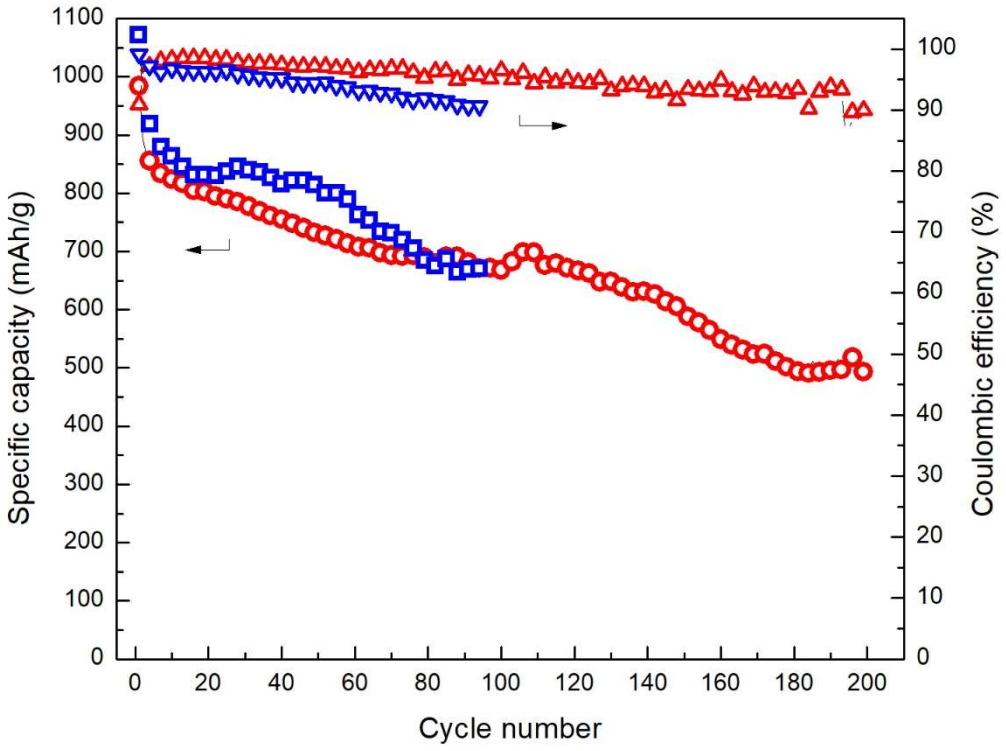

Figure 21. Cycle test of CZ/HPC and HPC. Blue: HPC. Red: CZ/HPC.

The cycle test of HPC and CZ/HPC based lithium sulfur battery is shown in Fig. 21. The charging rate is 0.2C and the batteries are charged to 2.6V and discharged to 1.8V. The first cycle specific capacity of CZ/HPC is around 980 mAh g^{-1} compare to 1060 mAh g^{-1} of HPC. The large amount of mesopores structure in HPC improve the utilization of sulfur which reflect to the high first cycle specific capacity of the battery.

However, the HPC battery fails at 97th cycle due to the poor reversible of the reaction. As for CZ/HPC, the injection of cobalt nanoparticles which immobilize the polysulfide ions effectively limits the shuttle effect and improve the cycle life of the battery. Compare with HPC in the first 97 cycles, the Coulombic efficiency of CZ/HPC battery is higher and more stable. The fading rate of CZ/HPC is 0.27 mAh g^{-1} per cycle which is lower than HPC with 0.31 mAh g^{-1} per cycle. Because of the strong polysulfide absorption ability which provided by cobalt nanoparticles, the fading rate is minished and the cycle life of the battery is extended to 150 cycles compare to 97 cycles for HPC.

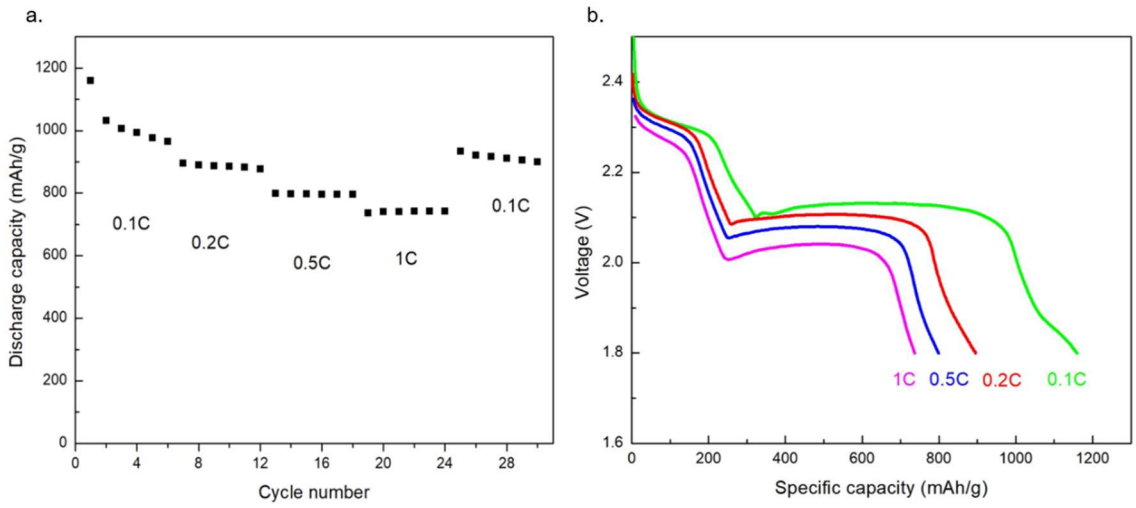

Figure 22: Rate test of CZ/HPC coin cell. (a). Specific capacity of the battery under different charging rate. (b). Voltage profile of discharge under different charging rate.

As for the rate test, the CZ/HPC battery is charged and discharged from 0.1C, 0.2C, 0.5C and 1C as shown in Fig. 22 (a).The specific capacity under different rate is stabilized around 1000 mAh g^{-1}, 900 mAh g^{-1}, 800 mAh g^{-1} and 750 mAh g^{-1} respectively After the 1C test, the battery again cycled under 0.1C in order to prove the saleability of the electrode after high rate charge and discharge. The capacity remains the same after 1C cycling which shows the resistance of the battery under high charging rate. The discharge

profile is shown in Fig. 22 (b). Both plateaus are shown in the discharge curve which prove the completion of the reaction. The 1C rate test shows excellent rate capability and outstanding ion transfer ability of the electrode which maintain the voltage of the discharge plateau under high rate.

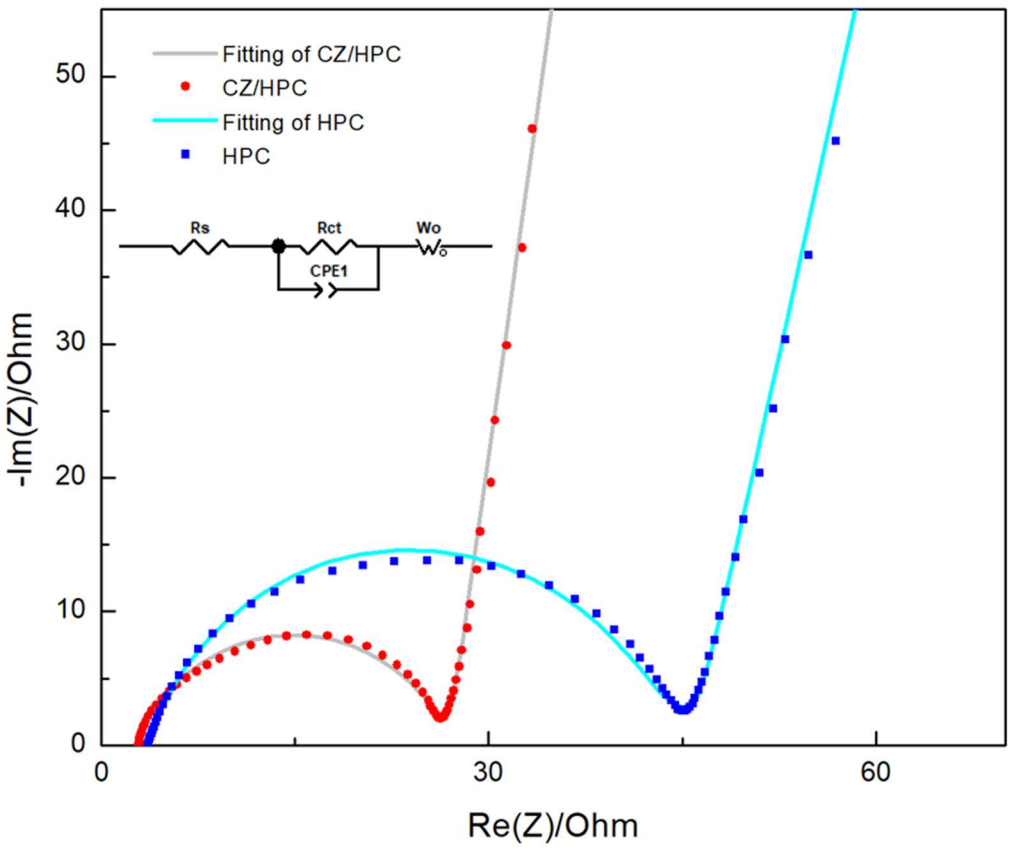

Figure 23. Nyquist plot of EIS.

	CZ/HPC	HPC
	Resistance (Ohm)	
R (internal resistance)	2.87	3.72
R_s (interfacial resistance)	2.68	3.48
R_{ct} (charge transfer resistance)	24.24	39.65

Table 2: Simulation result of Nyquist plot

The Nyquist plot of EIS data is shown in Fig. 23 and EC lab software is used to analyze the data. The fitting modal is demonstrated on the figure while the curve fitted the data and the error between is ignorable. Table. 2 Present the internal resistance (R), interfacial resistance (R_s) and charge transfer resistance (R_{ct}). The internal resistance of CZ/HPC coin cell is 2.87 Ohm which is slightly lower compare with 3.72 Ohm for HPC. The charge transfer resistance of CZ/HPC is lower than HPC as shown as 24.24 and 39.65 respectively. These is because of the injection of cobalt nanoparticles which increase the conductivity of the material. Electrical resistivity of cobalt metal is 62.4 nΩ·m compare with around 3E-5 Ω·m for carbon material depend on the calcination temperature and crystal structure. because of the well distribution of cobalt nanoparticles over the HPC structure, the over all conductivity of the particle is decreased. As for the interfacial resistance, the value of CZ/HPC coin cell is 2.68 while the R_{int} of HPC is 3.48. This may due to the nitrogen doped carbon and nanopores generated from the calcination of 2-Methylimidazole. The injection of nitrogen atoms and the nano-porous structure improve the wetting of electrode by the DOL/DME electrolyte and further decrease the interfacial resistance.

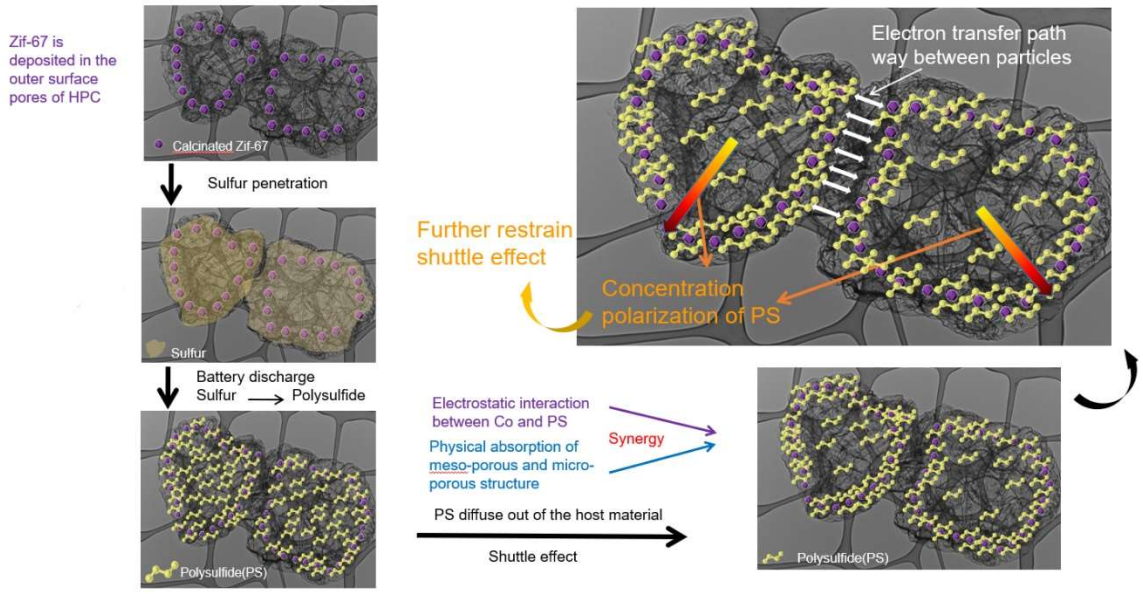

Figure 24: Sulfur absorption mechanism of CZ/HPC in the electrode.

Fig. 24 shows the proposed mechanism of S@CZ/HPC describing the effect of cobalt metal in stabilizing sulfur stored within the electrode. Cobalt nanoparticles are injected in HPC while these particles are immobilized in the porous structure and form a spherical layer (particle ring). As for S@CZ/HPC, sulfur is mixed with CZ/HPC and it is well dispersed all over the particle. During the discharge of the battery, on the first plateau of the discharge curve, sulfur is reduced to soluble polysulfide, and due to the low concentration of polysulfide in the electrolyte, the polysulfide tends to diffuse out of the particle and shuttle toward the anode. However, because of the excellent absorption ability of cobalt nanoparticles in the porous structure, the polysulfide largely retained within the pores during discharge and create a concentration polarization from the cobalt sphere to the center of the particle (concentration of polysulfide in the center of the particle is lower than which in the cobalt decorated mesoporous structure). This

phenomenon is like pack polysulfide into a sealed box which immobilized the soluble active material and limit the shuttle effect.

4.7. High loading test

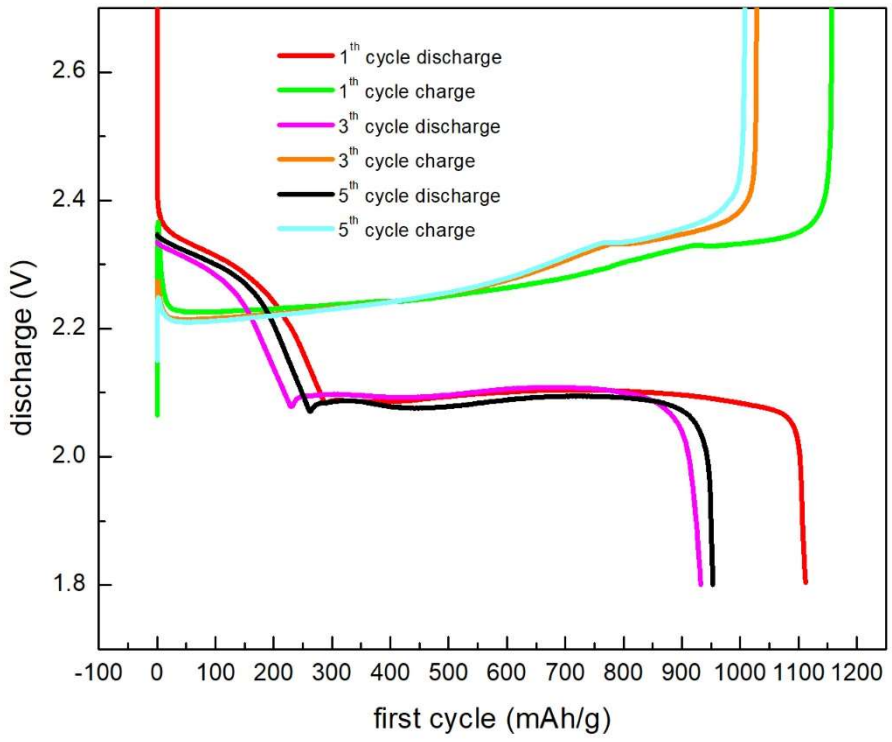

Figure 25: Charge and discharge profile of ultra high loading lithium sulfur battery with CZ/HPC electrode.

Ultra high loading, over 10 mg cm^{-2} surface loading of sulfur, lithium sulfur battery is assembled with S@CZ/HPC. To synthesis high loading electrode, large amount of active material needs to be formed on the aluminum foil which means to enlarge the thickness of the electrode. However, the increase of thickness brings up many issues. First, the ion transfer ability of the electrode is poor, because the electrolyte is difficult to reach the inner layer of the electrode. Second, in the electrode synthesis step, vaporize of water may cause the cracking of the electrode due to the surface tension and thicker

electrode has higher risk of cracking. In addition, the particle size is also very important for the fabrication of the electrode. If the particle size is too small, more binder needs to be added in the slurry to ensure the coverage over the high surface area. For S@CZ/HPC, because the sulfur loading in the host material is very high, the thickness of the electrode is relatively low, and the electrode can be fabricated without cracking. In addition, the size of the CZ/HPC particles are around 3.5-4 microns which is proper for the high loading electrode making and the weight percentage of binder in the electrode maintain the same compare with the 4 mg cm^{-2} loading batteries. As for the battery test, because of the poor ion conductivity, the charging rate is set to be 0.05C. The galvanic charge and discharge profile are shown in Fig. The specific capacity of the first cycle is around 1120 mAh g^{-1} and it fade to around 940 mAh g^{-1} at 5^{th} cycle. The first cycle capacity is relatively high while the cycle ability of the high loading battery is limited. The decrease in the length of the first plateau (which relates to the reduction of S_8 to high ordered polysulfides) from the 1^{st} and 2^{nd} cycle indicates that the main reason of the capacity fade may be caused by the reaction of polysulfide and lithium on the surface of the lithium metal anode. This reaction forms a Li_2S layer on the anode and prevent the direct contact between the lithium and the electrode. Because of the high polysulfide concentration in the electrolyte, the rate of this reaction is faster which strongly decreases the utility of sulfur.

5. Conclusion

In this project, a novel cobalt decorated hierarchical porous carbon sphere is developed. The material is synthesized by using spray dry method and NaCl as template. Insitu-synthesize method is used to form ZIF-67 particles and further generate cobalt nanoparticles in the carbon sphere. This synthesize method is friendly to industry which make the material has the potential to be commercialized. SEM and TEM images are shown to prove the successfully synthesis of the material and the morphology of NaCl@Gelatin, HCP and CZ/HPC are demonstrated. The size of the particles is measured through these images and the hierarchical pore size are also identified. XRD spectrum is analyzed to prove the existence of cobalt metal and the size of the nanoparticles. In addition, by analyze BET data, the surface area of HPC and CZ/HPC is found to be 535.1 m^2/g for HPC and 373.3 $m^2 g^{-1}$ for CZ/HPC. With BJH analysis, the pore size distribution is also demonstrated. Abundant mesopores are founded in both HPC and CZ/HPC. TGA and ICP data measure the cobalt weight percentage of in CZ/HPC and both characterization method provides the same value which is around 34.5%. The amount of sulfur inside the S@CZ/HPC is measured by TGA which proved that the loss of sulfur in the synthesize process can be ignored. The polysulfide absorption ability is demonstrated by the Li_2S_6 absorption test while the injection of cobalt nanoparticles effectively limits the diffusion of polysulfide. The battery test including CV and EIS demonstrate the reaction property which identified the reaction and some crucial factors for example the charge transfer resistance and inner resistance. Batteries using CZ/HPC as host material can deliver over 1000 mAh g^{-1} of specific capacity under 0.1C and the charge and discharge rate of the battery can reach 1C while 80% of the capacity can be remained.

The cycle life of this battery is 200 cycles while over 600 mAh g^{-1} of specific capacity can be remained. Furthermore, ultra high loading of lithium sulfur battery is assembled due to the large amount of microporous structure in HPC and CZ/HPC. The battery which surface loading is over 10 mg/cm^2 produced over 1100 mAh g^{-1} specific capacity in the first cycle.

6. Future works and recommend research directions

As for the future work, so other characterization can be done to analyze other property of this material. For example, X-ray Photoelectron Spectroscopy can be used to analyze the nitrogen amount in the carbon material. High resolution TEM can further detect the crystal structure of cobalt nanoparticles. The particle size of HPC and CZ/HPC can be adjusted by switch to other kind of spray dry nozzle which can spray the solution to larger or smaller droplets. Other kind of salt may play the same role of template instead of NaCl for other reasons. For example, some salt can decompose under high temperature, so the washing step can be skip. the cycle life of the battery can be improved. Other effective polysulfide absorption materials can be used in the HPC such as metal oxide or metal sulfide.

Before the commercialize of lithium sulfur battery, other factors also need to be studied. The safety issue is one of the most important problem that need to be solved. The high activity of lithium metal anode is dangerous while exposed to air. Electrolyte for lithium sulfur battery also need further study because the DOL/DME electrolyte which is commonly used for lithium sulfur battery has higher cost compare to $LiPF_6$ electrolyte used in lithium ion batteries. To be used in electro-vehicles, the cycle life also needs to be improved. As for other factors, the electrolyte/active material ratio also need to be further studied. The reaction mechanism of lithium and sulfur which is important for catalyze of the reaction also need further research. For the type of cells, most of the research only use coin cells which is not practical. Larger-scale performance need to be further study by assemble pouch cells or cylindrical cells. In conclusion, the future research direction

should not be limited to the loading of the battery but focus on more practical factors which can promote the commercialize of lithium sulfur batteries.

7. References

(1) Karagiannopoulos, L. Tesla boom lifts Norway's electric car sales to record market share. https://www.reuters.com/article/us-norway-autos/tesla-boom-lifts-norways-electric-car-sales-to-58-percent-market-share-idUSKCN1RD2BB (accessed Aug 14, 2019).

(2) Fotouhi, A.; Auger, D. J.; Propp, K.; Longo, S.; Wild, M. A Review on Electric Vehicle Battery Modelling: From Lithium-Ion toward Lithium–Sulphur. *Renewable and Sustainable Energy Reviews***2016**, *56*, 1008–1021.

(3) Warner, J. T. Lithium-Ion Cell Manufacturing. *Lithium-Ion Battery Chemistries* **2019**, 219–252.

(4) Y. Xiang, J. Li, J. Lei, D. Liu, Z. Xie, D. Qu, K. Li, T. Deng, H. Tang, Advanced Separators for Lithium-Ion and Lithium–Sulfur Batteries: A Review of Recent **Progress** *ChemSusChem* **2016**, *9*, 3023.

(5) Ji, X.; Lee, K. T.; Nazar, L. F. A Highly Ordered Nanostructured Carbon–Sulphur Cathode for Lithium–Sulphur Batteries. *Nature Materials* **2009**, *8*(6), 500–506.

(6) Zhang, S. S. Liquid Electrolyte Lithium/Sulfur Battery: Fundamental Chemistry, Problems, and Solutions. *Journal of Power Sources* **2013**, *231*, 153–162.

(7) Wang, Q.; Jin, J.; Wu, X.; Ma, G.; Yang, J.; Wen, Z. A Shuttle Effect Free Lithium Sulfur Battery Based on a Hybrid Electrolyte. *Phys. Chem. Chem. Phys.* **2014**, *16*(39), 21225–21229.

(8) Xu, N.; Qian, T.; Liu, X.; Liu, J.; Chen, Y.; Yan, C. Greatly Suppressed Shuttle Effect for Improved Lithium Sulfur Battery Performance through Short Chain Intermediates. *Nano Letters* **2016**, *17*(1), 538–543.

(9) Busche, M. R.; Adelhelm, P.; Sommer, H.; Schneider, H.; Leitner, K.; Janek, J. Systematical Electrochemical Study on the Parasitic Shuttle-Effect in Lithium-Sulfur-Cells at Different Temperatures and Different Rates. *Journal of Power Sources* **2014**, *259*, 289–299.

(10) Bresser, D.; Passerini, S.; Scrosati, B. ChemInform Abstract: Recent Progress and Remaining Challenges in Sulfur-Based Lithium Secondary Batteries - A Review. *ChemInform* **2013**, *45*(1).

(11) Recent Developments and Future Prospects for Lithium Rechargeable Batteries. *Fuel and Energy Abstracts* **2002**, *43*(3), 193.

(12) Sun, Y.-K.; Lee, D.-J.; Lee, Y. J.; Chen, Z.; Myung, S.-T. Cobalt-Free Nickel Rich Layered Oxide Cathodes for Lithium-Ion Batteries. *ACS Applied Materials & Interfaces* **2013**, *5*(21), 11434–11440.

(13) Sakaebe, H. Lithium-Sulfur Batteries. *Encyclopedia of Applied Electrochemistry***2014**, 1197–1201.

(14) . M. Wild, L. O'Neill, T. Zhang, R. Purkayastha, G. Minton, M. Marinescu and G. J. Offer, *Energy Environ. Sci.*, 2015, **8**, 3477

(15) Peng, H.-J., Huang, J.-Q., Cheng, X.-B., Zhang, Q., *Adv. Energy Mater.* 2017, 7, 1700260.

(16) Sohn, H.; Gordin, M. L.; Xu, T.; Chen, S.; Lv, D.; Song, J.; Manivannan, A.; Wang, D. *ACS Applied Materials & Interfaces***2014**, *6*(10), 7596–7606.

(17) Jayaprakash, N.; Shen, J.; Moganty, S. S.; Corona, A.; Archer, L. A. *Angewandte Chemie International Edition***2011**, *50*(26), 5904–5908.

(18) Evers, S.; Nazar, L. F. *Chem. Commun.***2012**, *48*(9), 1233–1235.

(19) Zhang, X.-Q.; He, B.; Li, W.-C.; Lu, A.-H. Hollow Carbon Nanofibers with Dynamic Adjustable Pore Sizes and Closed Ends as Hosts for High-Rate Lithium-Sulfur Battery Cathodes. *Nano Research* **2018**, *11*(3), 1238–1246.

(20) Liang, X.; Kwok, C. Y.; Lodi-Marzano, F.; Pang, Q.; Cuisinier, M.; Huang, H.; Hart, C. J.; Houtarde, D.; Kaup, K.; Sommer, H.; Brezesinski, T.; Janek, J.; Nazar, L. F. *Advanced Energy Materials* **2015**, *6*(6), 1501636.

(21) Luo, D.; Li, G.; Deng, Y. P.; Zhang, Z.; Li, J.; Liang, R.; Li, M.; Jiang, Y.; Zhang, W.; Liu, Y.; Lei, W.; Yu, A.; Chen, Z. *Advanced Energy Materials* **2019**, *9*(18), 1900228.

(22) Zhang, Z.; Lai, Y.; Zhang, Z.; Zhang, K.; Li, J. *Electrochimica Acta* **2014**, *129*, 55–61.

(23) Shao, H.; Wang, W.; Zhang, H.; Wang, A.; Chen, X.; Huang, Y. *Journal of Power Sources* **2018**, *378*, 537–545.

(24) Zheng, G.; Lee, S. W.; Liang, Z.; Lee, H.-W.; Yan, K.; Yao, H.; Wang, H.; Li, W.; Chu, S.; Cui, Y. Interconnected Hollow Carbon Nanospheres for Stable Lithium Metal Anodes. *Nature Nanotechnology***2014**, *9*(8), 618–623.

(25) Zhang, Y.; Luo, W.; Wang, C.; Li, Y.; Chen, C.; Song, J.; Dai, J.; Hitz, E. M.; Xu, S.; Yang, C.; Wang, Y.; Hu, L. High-Capacity, Low-Tortuosity, and Channel-Guided Lithium Metal Anode. *Proceedings of the National Academy of Sciences***2017**, *114*(14), 3584–3589.

(26) Yan, K.; Lu, Z.; Lee, H.-W.; Xiong, F.; Hsu, P.-C.; Li, Y.; Zhao, J.; Chu, S.; Cui, Y. *Nature Energy***2016**, *1*(3).

(27) Yuan, L.; Yuan, H.; Qiu, X.; Chen, L.; Zhu, W. Improvement of Cycle Property of Sulfur-Coated Multi-Walled Carbon Nanotubes Composite Cathode for Lithium/Sulfur Batteries. *Journal of Power Sources* **2009**, *189* (2), 1141–1146.

(28) Wang, H.; Yang, Y.; Liang, Y.; Robinson, J. T.; Li, Y.; Jackson, A.; Cui, Y.; Dai, H. Graphene-Wrapped Sulfur Particles as a Rechargeable Lithium–Sulfur Battery Cathode Material with High Capacity and Cycling Stability. *Nano Letters* **2011**, *11*(7), 2644–2647.

(29) Zhou, G. , Pei, S. , Li, L. , Wang, D. , Wang, S. , Huang, K. , Yin, L. , Li, F. and Cheng, H. (2014), A Graphene–Pure-Sulfur Sandwich Structure for Ultrafast, Long-Life Lithium–Sulfur Batteries. Adv. Mater., 26: 625-631.

(30) Wang, M.; Zhang, H.; Wang, Q.; Qu, C.; Li, X.; Zhang, H. Steam-Etched Spherical Carbon/Sulfur Composite with High Sulfur Capacity and Long Cycle Life for Li/S Battery Application. *ACS Applied Materials & Interfaces* **2015**, *7* (6), 3590–3599.

(31) Zhang, B.; Lai, C.; Zhou, Z.; Gao, X. Preparation and Electrochemical Properties of Sulfur–Acetylene Black Composites as Cathode Materials. *Electrochimica Acta* **2009**, *54*(14), 3708–3713.

(32) Choi, Y.-J.; Kim, K.-W.; Ahn, H.-J.; Ahn, J.-H. Improvement of Cycle Property of Sulfur Electrode for Lithium/Sulfur Battery. *Journal of Alloys and Compounds* **2008**, *449*(1-2), 313–316.

(33) Shi, H.; Lv, W.; Zhang, C.; Wang, D.-W.; Ling, G.; He, Y.; Kang, F.; Yang, Q.-H. Functional Carbons Remedy the Shuttling of Polysulfides in Lithium-Sulfur

Batteries: Confining, Trapping, Blocking, and Breaking Up. *Advanced Functional Materials* **2018**, *28*(38), 1800508.

(34) Pang, Q.; Nazar, L. F. Long-Life and High-Areal-Capacity Li–S Batteries Enabled by a Light-Weight Polar Host with Intrinsic Polysulfide Adsorption. *ACS Nano* **2016**, *10* (4), 4111–4118.

(35) Pang, Q.; Liang, X.; Kwok, C. Y.; Kulisch, J.; Nazar, L. F. A Comprehensive Approach toward Stable Lithium-Sulfur Batteries with High Volumetric Energy Density. *Advanced Energy Materials* **2016**, *7* (6), 1601630.

(36) Liu, J.; Li, W.; Duan, L.; Li, X.; Ji, L.; Geng, Z.; Huang, K.; Lu, L.; Zhou, L.; Liu, Z.; Chen, W.; Liu, L.; Feng, S.; Zhang, Y. A Graphene-like Oxygenated Carbon Nitride Material for Improved Cycle-Life Lithium/Sulfur Batteries. *Nano Letters* **2015**, *15* (8), 5137–5142.

(37) Li, G.; Lei, W.; Luo, D.; Deng, Y.-P.; Wang, D.; Chen, Z. 3D Porous Carbon Sheets with Multidirectional Ion Pathways for Fast and Durable Lithium-Sulfur Batteries. *Advanced Energy Materials* **2017**, *8*(8), 1702381.

(38) Ma, Y.; Zhang, H.; Wu, B.; Wang, M.; Li, X.; Zhang, H. Lithium Sulfur Primary Battery with Super High Energy Density: Based on the Cauliflower-like Structured C/S Cathode. *Scientific Reports* **2015**, *5*(1).

(39) Xu, G.; Ding, B.; Shen, L.; Nie, P.; Han, J.; Zhang, X. Sulfur Embedded in Metal Organic Framework-Derived Hierarchically Porous Carbon Nanoplates for High Performance Lithium–Sulfur Battery. *Journal of Materials Chemistry A* **2013**, *1* (14), 4490.

(40) Zheng, J.; Tian, J.; Wu, D.; Gu, M.; Xu, W.; Wang, C.; Gao, F.; Engelhard, M. H.; Zhang, J.-G.; Liu, J.; Xiao, J. Lewis Acid–Base Interactions between Polysulfides and Metal Organic Framework in Lithium Sulfur Batteries. *Nano Letters* **2014**, *14*(5), 2345–2352.

(41) Wu, H. B.; Wei, S.; Zhang, L.; Xu, R.; Hng, H. H.; Lou, X. W. D. Embedding Sulfur in MOF-Derived Microporous Carbon Polyhedrons for Lithium-Sulfur Batteries. *Chemistry - A European Journal* **2013**, *19*(33), 10804–10808.

(42) Bao, W.; Zhang, Z.; Qu, Y.; Zhou, C.; Wang, X.; Li, J. Confine Sulfur in Mesoporous Metal–Organic Framework @ Reduced Graphene Oxide for Lithium Sulfur Battery. *Journal of Alloys and Compounds* **2014**, *582*, 334–340.

(43) Bao, W.; Zhang, Z.; Zhou, C.; Lai, Y.; Li, J. Multi-Walled Carbon Nanotubes @ Metal–Organic Framework for Lithium Sulfur Battery. *Journal of Power Sources* **2014**, *248*, 570–576.

(44) Pang, Q.; Liang, X.; Kwok, C. Y.; Nazar, L. F. Advances in Lithium–Sulfur Batteries Based on Multifunctional Cathodes and Electrolytes. *Nature Energy* **2016**, *1*(9).

(45) Li, Z.; Li, C.; Ge, X.; Ma, J.; Zhang, Z.; Li, Q.; Wang, C.; Yin, L. Reduced Graphene Oxide Wrapped MOFs-Derived Cobalt-Doped Porous Carbon Polyhedrons as Sulfur Immobilizers as Cathodes for High Performance Lithium Sulfur Batteries. *Nano Energy* **2016**, *23*, 15–26.

(46) Goldstein, J.; Newbury, D. E.; Michael, J. R.; Ritchie, N. W. M.; Scott, J. H. J.; Joy, D. C. *Scanning electron microscopy and x-ray microanalysis*; Springer: New York, NY, 2018.

(47) *ELECTRON microscopy and analysis*; s.n., 1971.

(48) Reimer, L.; Kohl, H. *Transmission electron microscopy: physics of image formation*; Springer: New York, NY, 2010.

(49) Fultz, B.; Howe, J. M. *Transmission electron microscopy and diffractometry of materials: with numerous exercises*; Springer: Berlin, 2008.

(50) Kelly, P. M.; Jostsons, A.; Blake, R. G.; Napier, J. G. The Determination of Foil Thickness by Scanning Transmission Electron Microscopy. *Physica Status Solidi (a)***1975**, *31*(2), 771–780.

(51) Warren, B. E. *X-ray diffraction*; Dover Publications: New York, 2014.

(52) Guinier André; Lorrain, P.; Lorrain Dorothée Sainte-Marie. *X-ray diffraction: in crystals, imperfect crystals, and amorphous bodies*; Dover Publications: New York, 2000.

(53) Holzwarth, U.; Gibson, N. The Scherrer Equation versus the Debye-Scherrer Equation. *Nature Nanotechnology***2011**, *6*(9), 534–534.

(54) Derivation of The Bragg Scattering Law. *Introduction to Modern Physics***1983**, 686–689.

(55) Guillong, M.; Günther, D. Effect of Particle Size Distribution on ICP-Induced Elemental Fractionation in Laser Ablation-Inductively Coupled Plasma-Mass Spectrometry. *J. Anal. At. Spectrom.***2002**, *17*(8), 831–837.

(56) Ravikovitch, P. I.; Neimark, A. V. Characterization of Nanoporous Materials from Adsorption and Desorption Isotherms. *Colloids and Surfaces A: Physicochemical and Engineering Aspects***2001**, *187-188*, 11–21.

(57) Gelb, L. D.; Gubbins, K. E. Characterization of Porous Glasses: Simulation Models, Adsorption Isotherms, and the Brunauer−Emmett−Teller Analysis Method. *Langmuir***1998**, *14*(8), 2097–2111.

(58) Gelb, L. D.; Gubbins, K. E. Pore Size Distributions in Porous Glasses: A Computer Simulation Study. *Langmuir***1999**, *15*(2), 305–308.

(59) Olivier, J. P. Modeling Physical Adsorption on Porous and Nonporous Solids Using Density Functional Theory. *Journal of Porous Materials***1995**, *2*(1), 9–17.

(60) Gor, G. Y.; Thommes, M.; Cychosz, K. A.; Neimark, A. V. Quenched Solid Density Functional Theory Method for Characterization of Mesoporous Carbons by Nitrogen Adsorption. *Carbon***2012**, *50*(4), 1583–1590.

(61) Nicholson, R. S. Theory and Application of Cyclic Voltammetry for Measurement of Electrode Reaction Kinetics. *Analytical Chemistry***1965**, *37*(11), 1351–1355.

(62) Kendig, M. W.; Scully, J. R.; Silverman, D. C. *Electrochemical impedance: analysis and interpretation*; ASTM: Place of publication not identified, 1993.

(63) Tompkins, H. G.; Augis, J. A. The Oxidation of Cobalt in Air from Room Temperature to 467°C. *Oxidation of Metals* **1981**, *16*(5-6), 355–369.

(64) Ling, M.; Zhang, L.; Zheng, T.; Feng, J.; Guo, J.; Mai, L.; Liu, G. Nucleophilic Substitution between Polysulfides and Binders Unexpectedly Stabilizing Lithium Sulfur Battery. *Nano Energy***2017**, *38*, 82–90.

(65) Ding, B.; Shen, L.; Xu, G.; Nie, P.; Zhang, X. Encapsulating Sulfur into Mesoporous TiO2 Host as a High Performance Cathode for Lithium–Sulfur Battery. *Electrochimica Acta***2013**, *107*, 78–84.

(66) Liang, X.; Liu, Y.; Wen, Z.; Huang, L.; Wang, X.; Zhang, H. A Nano-Structured and Highly Ordered Polypyrrole-Sulfur Cathode for Lithium–Sulfur Batteries. *Journal of Power Sources***2011**, *196*(16), 6951–6955.

(67) Balakumar, K.; Kalaiselvi, N. High Sulfur Loaded Carbon Aerogel Cathode for Lithium–Sulfur Batteries. *RSC Advances***2015**, *5*(43), 34008–34018.

(68) Agostini, M.; Scrosati, B.; Hassoun, J. An Advanced Lithium-Ion Sulfur Battery for High Energy Storage. *Advanced Energy Materials***2015**, *5*(16), 1500481.

(69) Song, J.; Yu, Z.; Gordin, M. L.; Wang, D. Advanced Sulfur Cathode Enabled by Highly Crumpled Nitrogen-Doped Graphene Sheets for High-Energy-Density Lithium–Sulfur Batteries. *Nano Letters***2016**, *16*(2), 864–870.